



Seismic characterization of Iranian strong motion stations in Kermanshah province (Iran) using single-station Rayleigh wave ellipticity inversion of ambient noise measurements

Iman Ashayeri¹ · Mohammad Pourmohammad Shahvar² · Amir Moghohfeie¹

Received: 1 November 2021 / Accepted: 17 February 2022 / Published online: 6 March 2022
© The Author(s), under exclusive licence to Springer Nature B.V. 2022

Abstract

Kermanshah province experienced the most recent destructive earthquake in Iran on 12 November 2017 with M_w 7.3. Although this event was recorded by most Iran Strong Motion Network (ISMN) stations in the province, unfortunately, the site conditions of most of these stations were not properly identified. This study investigates seventeen ISMN stations operational in Kermanshah province to characterize them using available geological maps and by analyzing ambient noise recorded at these stations. Ambient noise analyses are efficient and cost-effective methods for identifying resonance frequency and shear wave velocity profiles. Horizontal to vertical spectral ratio of microtremors (mHVSR), time–frequency analysis of horizontal to vertical components (HVTFA), and Random Decrement technique (RayDec) were used in this study. Given the geological lateral variability of ground structure, these ambient noise analyses, along with 1D-linear elastic seismic site response analyses, provide a clearer understanding of site conditions at these stations than the available PS-logs. This study presents site proxies describing the geometry of subsurface layers, mechanical characteristics, and resonance frequencies at these stations.

Keywords Strong motion station · Seismic characterization · Ambient noise analysis · Ellipticity inversion · Site proxies

✉ Iman Ashayeri
i.ashayeri@razi.ac.ir; iashayeri@yahoo.com

Mohammad Pourmohammad Shahvar
m.shahvar@bhrc.ac.ir

Amir Moghohfeie
amir.sana1390@gmail.com

¹ Earthquake Engineering, Civil Engineering Department, School of Engineering, Razi University, P.O. Box: 67149-67346, Kermanshah, Iran

² Engineering Seismology, Road, Housing and Urban Development Research Center, Tehran, Iran

1 Introduction

Strong ground motion networks are essential for many seismological and earthquake engineering investigations on local, regional, and global scales. However, knowing the geological settings, seismic characteristics, and geotechnical specifications of the stations are just as important as recording seismological events. For example, useful geological and geotechnical specifications are available from the Japanese strong motion network (K-NET and KiK-net) operated by the National Research Institute for Earth Science and Disaster Prevention (NIED) (<https://www.kyoshin.bosai.go.jp/>). More recently, Zhu et al. (2021) investigated 1742 K-NET and KiK-net earthquake recording stations to present an open-source site database comprising topographic and geological proxies inferred from regional models or maps. This database contains site characterization parameters such as average P and S-wave velocities, bedrock depths, and velocity contrast, as well as parameters obtained from earthquake horizontal to vertical spectral ratio (eHVSr) including peak frequency, amplitude, width, and prominence.

Although obtaining complete site information can be costly for governments and organizations operating seismological or strong motion networks, recent studies have revealed that it is crucial for each station, the site proxies to be available (Zhu et al. 2020). Applied more increasingly across the globe since the past decade, ambient noise analyses are very suitable and cost-efficient procedures for insight into the seismic characteristics of stations. Pilz et al. (2009) analyzed ambient noise at eight temporary seismological stations deployed in the northern part of Santiago, Chile, to investigate the resonance frequency and site amplification of the ground at these stations. Foti et al. (2011) investigated 37 stations of the Italian Accelerometric Archive (<http://itaca.mi.ingv.it>) using surface wave methods to identify the shear wave velocity profiles at these stations. They expressed the importance of seismic characterization of strong motion stations, and through their experimental results, they criticized the seismic classification at several stations of the Italian National Network. Di Giulio et al. (2012) explored surface wave dispersion inversion at 14 European strong motion stations within the NERIES EC-Project. Hobiger et al. (2013) applied inversions of Rayleigh wave ellipticity of ambient noise recorded at single stations during the NERIES EC-Project. They presented helpful guidelines for the reasonable identification of shear wave velocity structure from the joint inversion of Rayleigh wave ellipticity and other methods like multichannel analysis of surface waves and the spatial autocorrelation curve of ambient noise measurements. Through the InterPACIFIC project, Garofalo et al. (2016a, b) compared invasive and non-invasive methods for seismic site characterization. They compared surface wave methods as non-invasive methods with invasive methods of V_S and V_P measurements in boreholes. They concluded that a priori information, such as local geology, helps deal with the non-uniqueness of the solution of the inverse problem in surface wave methods and found that the variability of the results for both invasive and non-invasive methods was generally comparable.

Ashayeri et al. (2019, 2020) showed that a single site proxy that is time-averaged shear wave velocity to 30 m, namely $V_{S,30}$ is insufficient to characterize the local site effects of the Mw 7.3 earthquake on 12 November 2017 in Kermanshah, Iran. Ashayeri et al. (2020) applied various analyses on the ambient noise records at Sarpol-e-zahab city, Iran, after the Mw 7.3 earthquake. Their analyses identified the resonance frequency of the ground, competent bedrock depth, thickness of the top soil over engineering bedrock, $V_{S,30}$ and time-averaged shear wave velocity of soil layers above the engineering bedrock of the city. These findings were directly used by Ashayeri et al. (2021) to provide seismic microzonation of

Sarpol-e-zahab as well as urban scale offline shakemaps of the city related to the earthquake event. Recently, Cultrera et al. (2021) and Di Giulio et al. (2021) have expressed the importance of site characterization of seismic stations, considering seven indicators for characterizing site conditions, specifically fundamental resonance frequency, shear wave velocity profile, $V_{S,30}$, depth to both seismological and engineering bedrock, surface geology, and soil class.

The Iran Strong Motion Network (ISMN), operated by the Iranian Road, Housing, and Urban Development Research Center (BHRC, <https://ismn.bhrc.ac.ir/>) with about 1000 digital accelerograph stations, has been in service since 1992. Figure 1 shows the current geographic distribution of the stations over the country (Shahvar et al. 2021). This study focuses on the ISMN stations located in Kermanshah province in the west of Iran (see Fig. 2). The goal is to use ambient noise analysis to provide more information about the seismic characteristics and ground structure at some of these stations. With this aim, firstly, the geological setting of each station is discussed based on geological maps. Secondly, the V_s logs for each station from the seismic refraction tests of the ISMN database are presented. Thirdly, ambient noise recordings are analyzed using horizontal to vertical spectral ratio of microtremors (mHVSr), time–frequency analysis of horizontal to vertical components (HVTFA, Fäh et al. 2009), and Random Decrement technique (RayDec, Hobiger

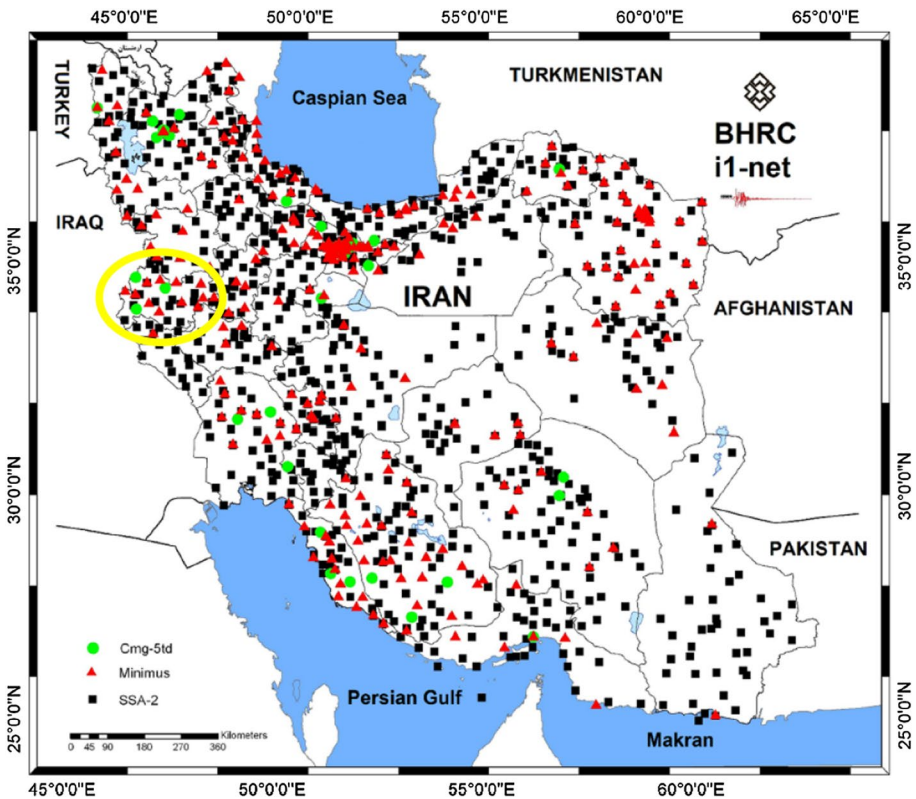


Fig. 1 The Iran Strong Motion Network (ISMN) (after Shahvar et al. 2021), yellow circle shows Kermanshah province

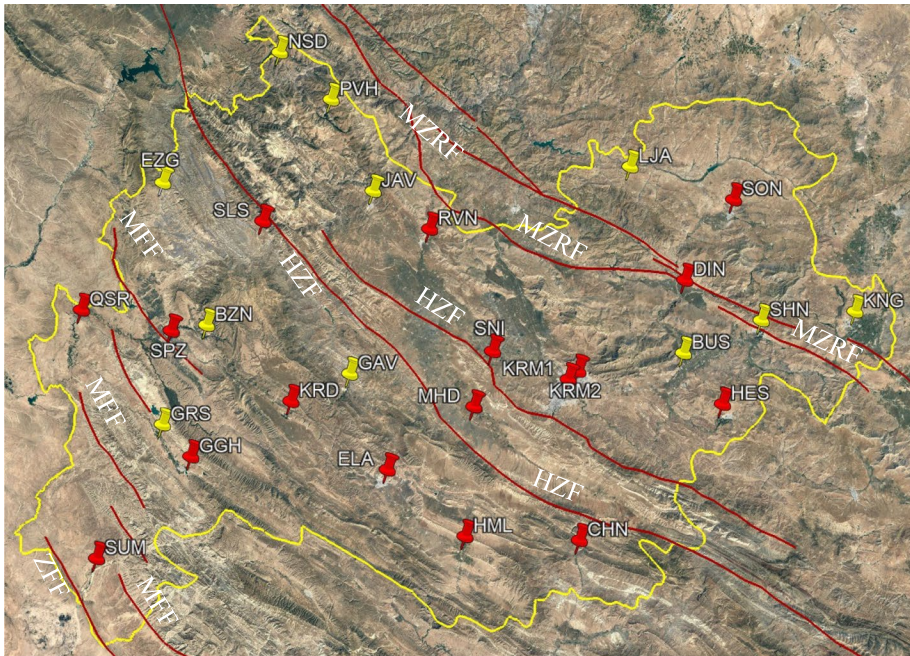


Fig. 2 ISMN stations in Kermanshah province and active faults of the region

et al. 2009) to present resonance frequency and ellipticity of Rayleigh waves, followed by applying velocity inversion of the ellipticity curve to obtain the shear wave velocity profile at each station. The analyses are followed by 1D-linear site response analysis of the shear wave velocity profiles at the stations. Finally, the results are discussed in terms of the site proxies of the stations.

2 ISMN stations in Kermanshah province

The ISMN operates in Kermanshah province with 27 stations, covering an area of about 25,000 square kilometers with about 1 station per 1000 square kilometers. The stations are located in cities of the province (Fig. 2). This study investigates the geological settings and seismic characteristics of the 17 stations that are shown in red in Fig. 2. The region is influenced by four active fault zones, namely Main Zagros Reverse Fault (MZRF), High Zagros Fault (HZF), Mountain Front Fault (MFF), and Zagros Foredeep Fault (ZFF) as shown in Fig. 2 (Hessami et al. 2003). Table 1 presents the approximate coordinates of these stations along with the maximum peak ground acceleration recorded, $V_{S,30}$ and the instrument type. It should be noted that BHRC reported $V_{S,30}$ for most of these stations based on the V_P and V_S measurements by seismic refraction tests, but mostly at far distance from the stations. Seismic refraction method is categorized as non-invasive seismic exploration that is based on the principles of seismic wave travelling through solid medium and the interface between two layers are identified by the refracted wave through the interface at different

Table 1 Location, records, site, and instrument type at ISMN stations examined in this study

Station	Urban area	Lat	Long	Max. PGA (date, Mw) (Gal)	V_{S30} (m/s) ^a	Instrument type
CHN	Chenar	33.928687°	47.120175°	32 (1998/10/04, 5.3)	419	SSA-2
DIN	Dinevar	34.583512°	47.447013°	81 (2017/11/12, 7.3)	514	SSA-2
ELA	Eslamabad-e-gharb	34.107891°	46.534968°	123 (2017/11/12, 7.3)	266	SSA-2
GGH	Gilan-e-gharb	34.137775°	45.933711°	56 (2013/11/22, 5.7)	692	SSA-2
HES	Hersin	34.270846°	47.558270°	5 (2017/11/12, 7.3)	NA	SSA-2
HML	Homeil	33.939623°	46.771787°	93 (2017/11/12, 7.3)	261	SSA-2
KRD	Kerend-e-gharb	34.280164°	46.240814°	261 (2017/11/12, 7.3)	800	SSA-2
KRM1	Kermanshah	34.335249°	47.087813°	55 (2017/11/12, 7.3)	NA	SSA-2
KRM2	Kermanshah	34.356459°	47.117347°	124 (2017/11/12, 7.3)	NA	SSA-2
MHD	Mahidasht	34.267110°	46.799196°	86 (2017/11/12, 7.3)	304	SSA-2
QSR	Qasr-e-shirin	34.505893°	45.591186°	NA	347	Guralp
RVN	Ravansar	34.714744°	46.663901°	120 (2017/11/12, 7.3)	267	SSA-2
SLS	Salas-e-babajani	34.733462°	46.151035°	799 (2018/08/25, 6)	281	SSA-2
SNI	Sarab-e-nilooфар	34.406971°	46.856411°	75 (2018/01/10, 4.7)	323	SSA-2
SON	Sonqor	34.785794°	47.598070°	50 (2002/04/24, 5.3)	1477	SSA-2
SPZ	Sarpol-e-zahab	34.455360	45.869850°	684 (2017/11/12, 7.3)	619	SSA-2
SUM	Sumar	33.876249°	45.644096°	406 (2018/01/11, 5.3)	642	SSA-2

^aReported by BHRC based on seismic refraction tests

velocity contrasts that is recorded by geophones at the ground surface. The measurements were performed by an ABEM-MK6 seismic system and 24 geophones laid out in a line.

3 Geological setting and ambient noise analysis

In this section, we present the geological settings, ground structure, and analysis of ambient noise recordings at each station. Geological maps with a scale of 1:100,000 from the Geological Survey of Iran (GSI, <https://www.gsi.ir/>) and the National Iranian Oil Company (NIOC, <https://www.nioc.ir/>) were used. Ambient noise was recorded with a broadband seismometer (r-sensor's CME-4111, frequency range of 0.033 to 50 Hz) and a 24-bit data

acquisition system at a rate of 200 samples per second for at least one hour next to the instrument of each station. The ambient noise records are preprocessed and analyzed by the Geopsy software (Wathelet et al. 2020) for determination of mHVSr, and HVTFA (Fäh et al. 2009), as well as the independent code for RayDec technique (Hobiger et al. 2009, and Github 2021), and the inversion of the ellipticity curve for determination of the shear wave velocity profile are performed using the Dinver framework by Wathelet (2008). Both HVTFA and RayDec methods try to extract ellipticity of Rayleigh wave from the three components of ambient noise. However, the mHVSr curve retrieved from spectral ratio of the horizontal components to the vertical component is contaminated by Love wave (Bonney-Claudet et al. 2008). To deal with retrieving ellipticity from mHVSr, the HVTFA method uses time–frequency representation of the vertical and the horizontal components by applying continuous Wavelet transform (CWT), and searches for the time of all maxima in the CWT of the vertical component and picks the CWT of horizontal components at each maximum with a quarter of period time-shift, then the ratio between the horizontal and vertical CWTs are calculated. The process is repeated for all frequencies to generate the ellipticity curve. Meanwhile, HVTFA may not be sufficiently effective when the contribution of other waves than Rayleigh wave increases at the same frequency band and time window (Fäh et al. 2009). In order to retrieve a more reliable ellipticity curve from mHVSr, the RayDec method applies random decrement technique to emphasize Rayleigh waves with respect to other wave types (i.e., Love and body waves). The RayDec method analyses the horizontal and vertical components in narrow frequency bands by applying narrow-band Chebyshev filter. Then, time for any changes in the sign from negative to positive of the vertical component is searched, and signals are buffered for the vertical component at the time of sign change and with a quarter of period time-shift for the horizontal components with a same length. The horizontal components are projected onto an axis of an azimuth. The algorithm searches for the azimuth angle at which the correlation between the buffered vertical and projected buffered horizontal signals is maximum. The ratio of the energies in the buffered signals weighted by the correlation factor is calculated as the ellipticity at the center frequency of the filter. The process is repeated by shifting the center frequency of the filter, covering the entire frequency range (Hobiger et al. 2009). In this way, RayDec not only shifts a quarter of period the time for the horizontal components, but also uses the maximum correlation factor between horizontal and vertical components to retrieve the ellipticity curve that is less contaminated by other waves.

As it was mentioned earlier, the ISMN has provided the shear wave velocity profiles for most of the stations, but they were measured at relatively large distance from the station. Hereby, we process the data with respect to geological lateral variability at the region, and then we use them to constrain the inversion of the ellipticity curve where appropriate. Furthermore, we have compared the peak frequency of the mHVSr curve with the first fundamental frequency of the theoretical horizontal spectral ratio of surface to bedrock motion (HSR) from 1D-linear modeling of the shear wave velocity profile elaborated in this study as well as the one provided by the ISMN database for each station. The HSR curve is calculated from the one dimensional linear elastic site response analysis of the V_s profile consisting of soil layers on top of an elastic half-space with the mechanical specification of the bedrock where it was available. The site response analyses were performed by DEEPSOIL v6.1, a well-known 1D wave propagation analysis program developed by Hashash et al. (2016). In this process, ambient noise analyses are carefully utilized to fill the shortage in site proxies for the stations of this study. Detailed analyses of each station are provided below.

3.1 Station CHN

Figure 3a presents the location of this station on the geological map of the region. The station is located on the edge of the Amiran and Taleh Zang Formations from the Eocene–Paleocene era. The Amiran Formation is composed of dark mudstone-siltstone layers (Homke et al. 2009). Observation of a geological section about 10 km southeast of the station shows a thickness of less than 1 km for the Amiran Formation, which stretches northeast beneath the Taleh Zang Formation. Therefore, it is inferred that the Amiran Formation best represents the geological setting of the CHN station. Figure 3c also presents the V_S -profile provided by the ISMN database approximately 137 m east of the station’s location. This is rather important because results could be affected by Quaternary era deposits at the logging location. Nevertheless, the V_S -profile shows a relatively loose layer ($V_S = 169$ m/s, probably from Quaternary deposits) on top of two layers with clear velocity contrasts at 4.2 m and 16.9 m with $V_S = 550$ and 709 m/s, respectively. It is not clear how deep the third layer extends, but based on its V_S , it is comparatively considered engineering

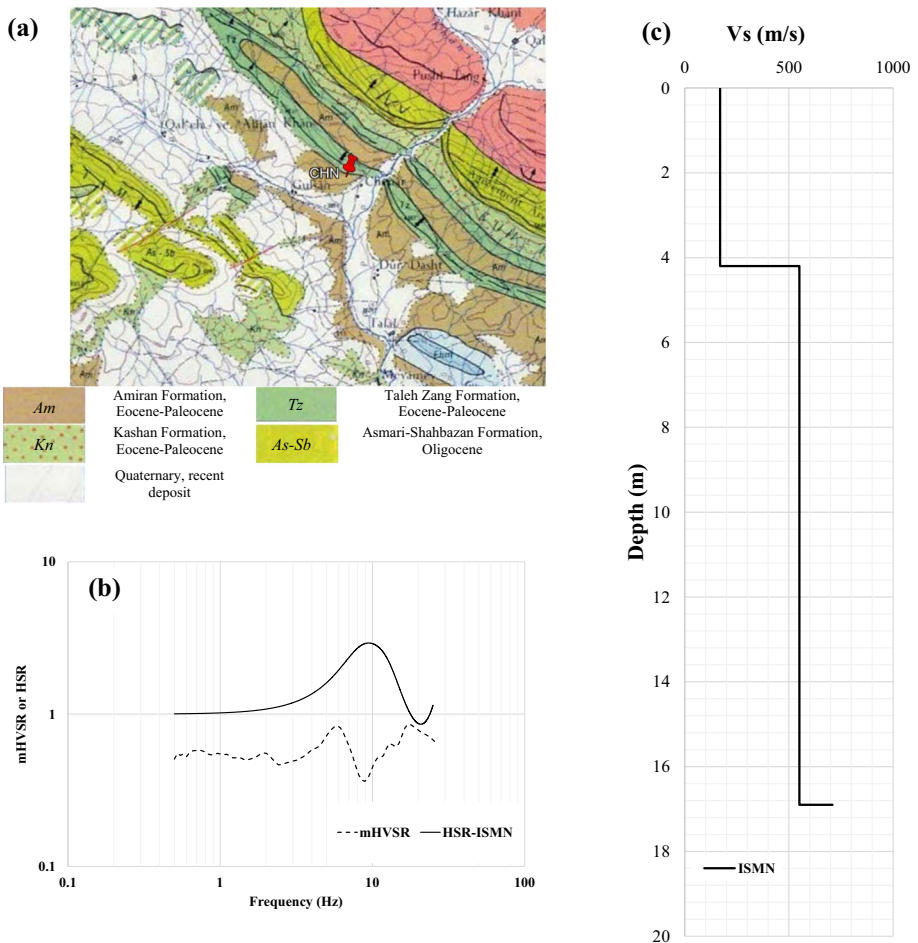


Fig. 3 Summary of CHN Station: a Geological map, b mHVSr and HSR curves, c V_S -profile

bedrock ($V_S=750$ m/s). Figure 3b presents the mHVSR of the ambient noise recorded at this station. The mHVSR curve does not show a clear peak with an amplitude of more than 1. Hence, a reliable ellipticity curve cannot be calculated for this station. Even so, the amplitude of the mHVSR curve shows a local maximum at 5.8 Hz (± 0.6). Furthermore, Fig. 3b shows the HSR curve calculated from the V_S -profile of Fig. 3c, which presents a peak of amplitude at 9.5 Hz. The authors conclude that a more representative V_S -profile of the station should be measured in the future by either direct borehole tests next to the station or more complex ambient noise and strong motion inversion methods.

3.2 Station DIN

Figure 4a presents the location of this station on the geological map of the region. The station is located on unconsolidated, texturally variable recent clastic deposits of the Quaternary era. Figure 4d presents the V_S -profile provided by the ISMN database approximately 10 m west of the location of the station. The V_S -profile shows relatively stiff ground ($V_S=276$ m/s) on top of two layers with clear velocity contrasts at 8.0 m and 21.7 m with $V_S=609$ and 1193 m/s, respectively. It is unclear how deep the third layer extends, but its V_S is considerably larger than that of engineering bedrock ($V_S=750$ m/s).

Figure 4b summarizes all ambient noise analyses of this station. The spectral ratio of microtremors, mHVSR, at Station DIN is shown in Fig. 4b along with the HSR from the ISMN V_S -profile (consisting of two layers resting over an elastic half-space with $V_S=1193$ m/s). The frequency of the peak amplitude of the mHVSR is 1.4 Hz (± 0.2), while the peak amplitude of the HSR of the ISMN profile is 6.4 Hz. The ellipticity curve of Rayleigh waves from ambient noise using HVTFa is presented in Fig. 4c along with the result of the least misfit curve obtained from inversion of the ellipticity curve. The initial models for inversion are constrained to the ISMN V_S -profile at the first and second layers, while the third layer's V_S and thickness are not constrained. As observed in Fig. 4c, the ellipticity of the least misfit model (the red line in Fig. 4c) properly fits to the observed ellipticity curve from ambient noise for a wide range of frequencies (i.e., 1 to 20 Hz). Moreover, the V_S -profile of the least misfit model is shown in Fig. 4d, and the HSR of the least misfit model is plotted in Fig. 4b for comparison with the ISMN V_S -profile and HSR, respectively. Figure 4b shows that the lowest frequency of the peak amplitude of HSR for the least misfit model is 1.5 Hz, which is very close to the peak frequency of mHVSR. Inspecting Fig. 4d reveals that the ISMN V_S -profile is relatively consistent with the inverted profiles at the top 20 m but does not present reasonable depths for engineering bedrock that is about 40 m. It should be noted that RayDec method was used to retrieve the ellipticity curve at this station as is shown in Fig. 4c along with the other ellipticity curves, but the length of the recorded signal was not adequately enough to retrieve a reliable ellipticity curve by RayDec method. Hence, the retrieved ellipticity was not used for velocity inversion analysis.

3.3 Station ELA

Figure 5a presents the location of this station on the geological map of the region on the alluvial plain and terraces of the Quaternary era. Figure 5d presents the V_S -profile provided in the ISMN database approximately 414 m southeast of the station's location. Although it is rather far away, there is no variation in the geological setting even at such a distance. The V_S -profile shows a loose 4.6 m thick layer ($V_S=104$ m/s) on top of a stiffer layer down to a

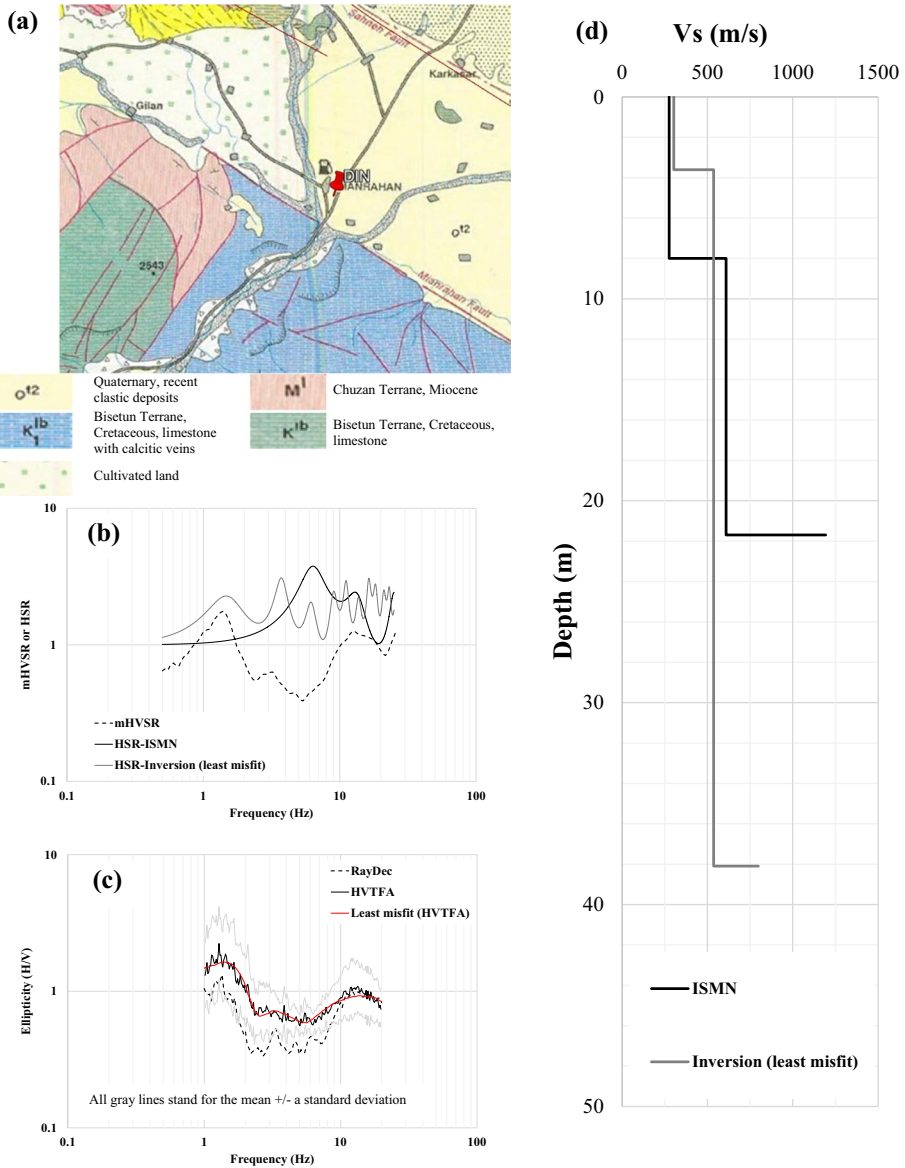


Fig. 4 Summary of DIN Station: **a** Geological map, **b** mHVSr and HSR curves, **c** ellipticity curves of ambient noise by HVTFA & RayDec methods as well as the least misfit model, **d** V_S -profiles

depth of 18.5 m ($V_S = 370$ m/s), which overlays a layer with $V_S = 636$ m/s. It is unclear how deep the third layer extends, and the V_S resembles weathered rock or very stiff soil looser than engineering bedrock ($V_S = 750$ m/s). Figure 5b presents the ambient noise analyses of the station. It shows that the frequency of the peak amplitude of mHVSr is at 1.1 Hz (± 0.2), which is consistent with the fact that the station is located on alluvial deposits from the Quaternary era (Fig. 5a). However, the V_S -profile from the ISMN database at this

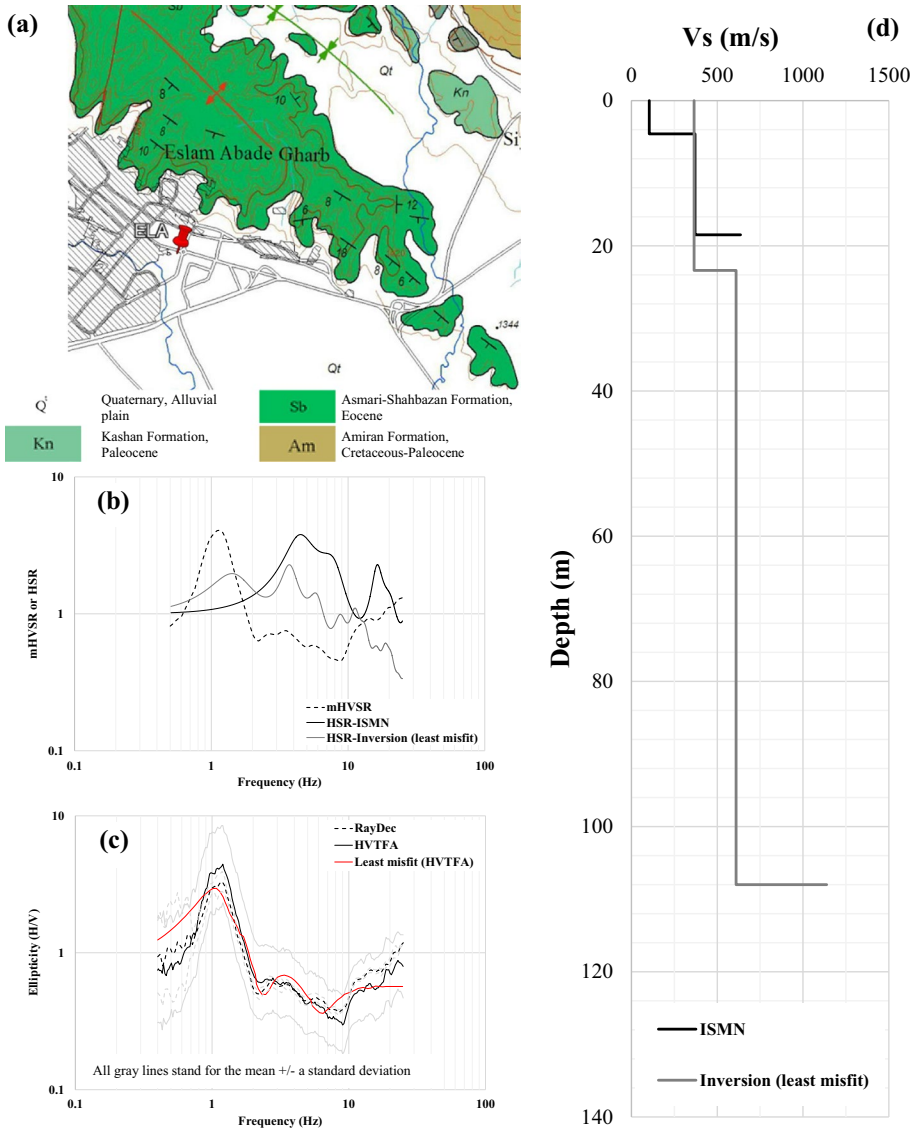


Fig. 5 Summary of ELA station: **a** Geological map, **b** mHVSr and HSR curves, **c** ellipticity curves of ambient noise by RayDec & HVTFA as well as the least misfit model, **d** V_s -profiles

station did not end in a layer suitably comparable with engineering bedrock. Nevertheless, Fig. 5b plots the HSR curve of the ISMN profile by considering the first two layers resting on the third layer as an elastic half-space, and it presents the peak frequency at 4.6 Hz, which is clearly inconsistent with the peak of mHVSr. The ellipticity of Rayleigh waves calculated from HVTFA and RayDec methods are shown in Fig. 5c. There is a good agreement between the ellipticity curves retrieved from the two methods. Figure 5c presents the ellipticity of the least misfit model of inversion analysis, which appropriately matches with

the both ellipticity curves, and more interestingly with the one of RayDec method. Figure 5d presents V_S -profiles of the least misfit model along with the ISMN profile, showing that the profile is relatively consistent with the least misfit model at the top 20 m. However, the least misfit model reveals that the competent bedrock could be located at a depth of about 110 m with $V_S = 1138$ m/s. Figure 5b plots the HSR curve for the least misfit model that shows the lowest frequency of the peak amplitude at 1.4 Hz, clearly matching the peak frequency from mHVSR.

3.4 Station GGH

Figure 6a presents the location of this station on the geological map of the region on the coarse and fine alluvium of the Quaternary era. Figure 6c presents the V_S -profile provided in the ISMN database approximately 160 m east of the station’s location. The

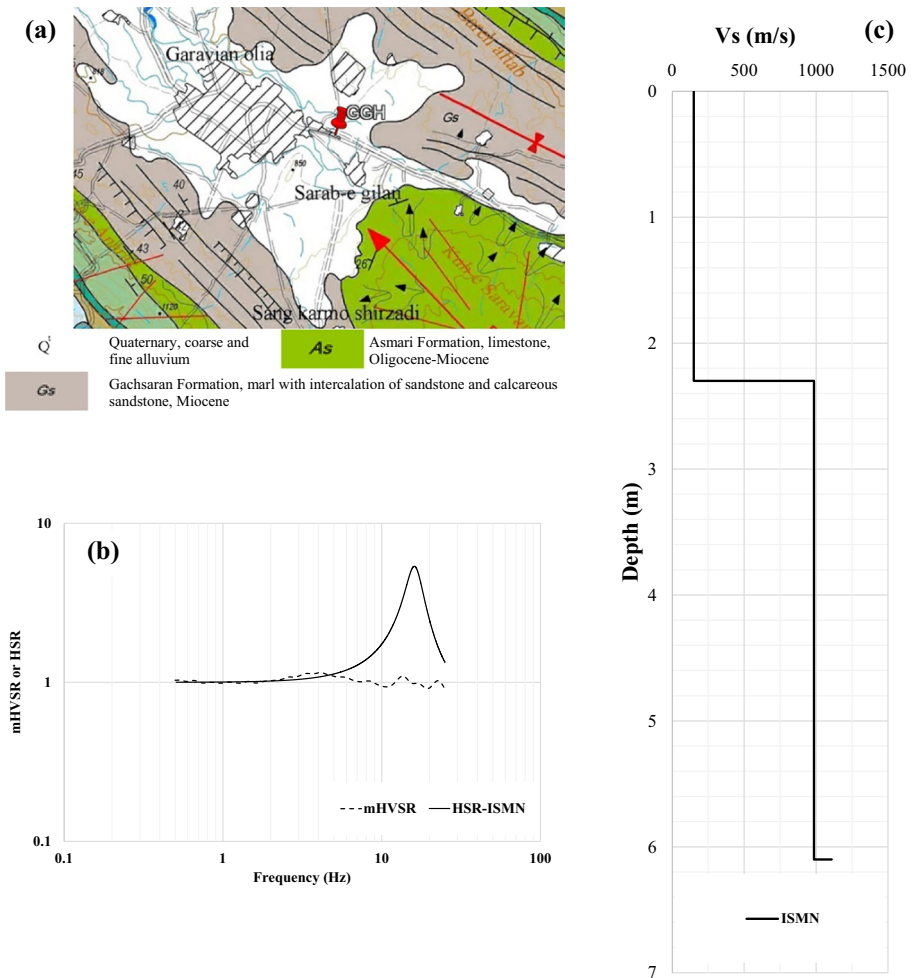


Fig. 6 Summary of GGH Station: **a** Geological map, **b** mHVSR and HSR curves, **c** V_S -profile

V_S -profile shows a relatively loose layer 2.3 m thick ($V_S=150$ m/s) on top of a layer with sharp velocity contrast ($V_S=986$ m/s) down to a depth of 6.1 m, which overlays a layer with $V_S=1108$ m/s. This profile reveals that the Quaternary alluvium is shallow, and the shear wave velocity of the second layer sharply exceeds the value of engineering bedrock ($V_S=750$ m/s). Figure 6b presents a flat mHVSr curve of the recorded ambient noise at GGH. This clearly confirms that the high V_S layers are too shallow at this station. Figure 6b also presents the HSR curve of the ISMN V_S -profile, showing a peak amplitude of 16 Hz. The authors conclude that GGH is placed on a rock site, and the ISMN V_S -profile is proportionally appropriate.

3.5 Station HES

Figure 7a presents the location of this station on the geological map of the region on the low level and young terrace of the Quaternary era. Unfortunately, the ISMN database does not provide a V_S -profile for this station. However, the geological map suggests that the recent Quaternary deposits at this station should not be deep. Figure 7b presents the ambient noise analyses of this station. It shows that the frequency of the peak amplitude of mHVSr is at 13.0 Hz (± 0.7), which is consistent with the fact that this station is located on thin alluvial deposits of the Quaternary era (Fig. 7a). Figure 7c shows the ellipticity of Rayleigh waves from HVTFA and RayDec methods, which are similar at frequencies higher than 10 Hz, but different at lower frequencies. Both ellipticity curves are used for velocity inversion and the least misfit models of the inversion analyses are plotted in Fig. 7c. The comparison of the ellipticity curves of the least misfit models reveals the peak and right flank of the ellipticity curve are better modelled in the inversion of the ellipticity curve of RayDec method. Figure 7b plots the HSR curves for the least misfit models, showing the lowest frequency of the peak amplitude at 11.8 and 14.3 Hz for the two least misfit ellipticity curves of HVTFA and RayDec methods, respectively. Although both HSR curves appropriately represent the peak frequency of mHVSr, the HSR curve of the least misfit model of the ellipticity of RayDec method is more consistent with the peak frequency of mHVSr. Figure 7d presents V_S -profiles of the least misfit models. They demonstrate that the top layer is thin (1 to 3 m), covering relatively thin, very stiff soil or weathered rock (thickness of about 10 m) with $V_S=579$ to 634 m/s. The third layer is identified as competent bedrock with $V_S=1100$ to 1275 m/s.

3.6 Station HML

Figure 8 presents the location of this station on the geological map of the region. The station is located on recent deposits from the Quaternary era. Figure 8d presents the V_S -profile provided in the ISMN database approximately 161 m southwest of the station's location. The V_S -profile shows a relatively loose layer 6.1 m thick ($V_S=170$ m/s) on top of a relatively stiff layer with $V_S=302$ m/s down to a depth of 23.1 m that overlays a sharp velocity contrast with $V_S=900$ m/s. The shear wave velocity of the third layer resembles engineering bedrock. Figure 8b summarizes all ambient noise analyses of this station. The spectral ratio of microtremors, mHVSr, for HML is shown in Fig. 8b along with the HSR from ISMN's V_S -profile (see Fig. 8d, consisting of two layers resting over an elastic half-space with $V_S=900$ m/s). The frequency of the peak amplitude of mHVSr is 1.9 Hz (± 0.3), while the peak amplitude of the HSR of the ISMN profile is 3.2 Hz. The ellipticity curve of Rayleigh waves from HVTFA of ambient noise is presented in Fig. 8c along with the

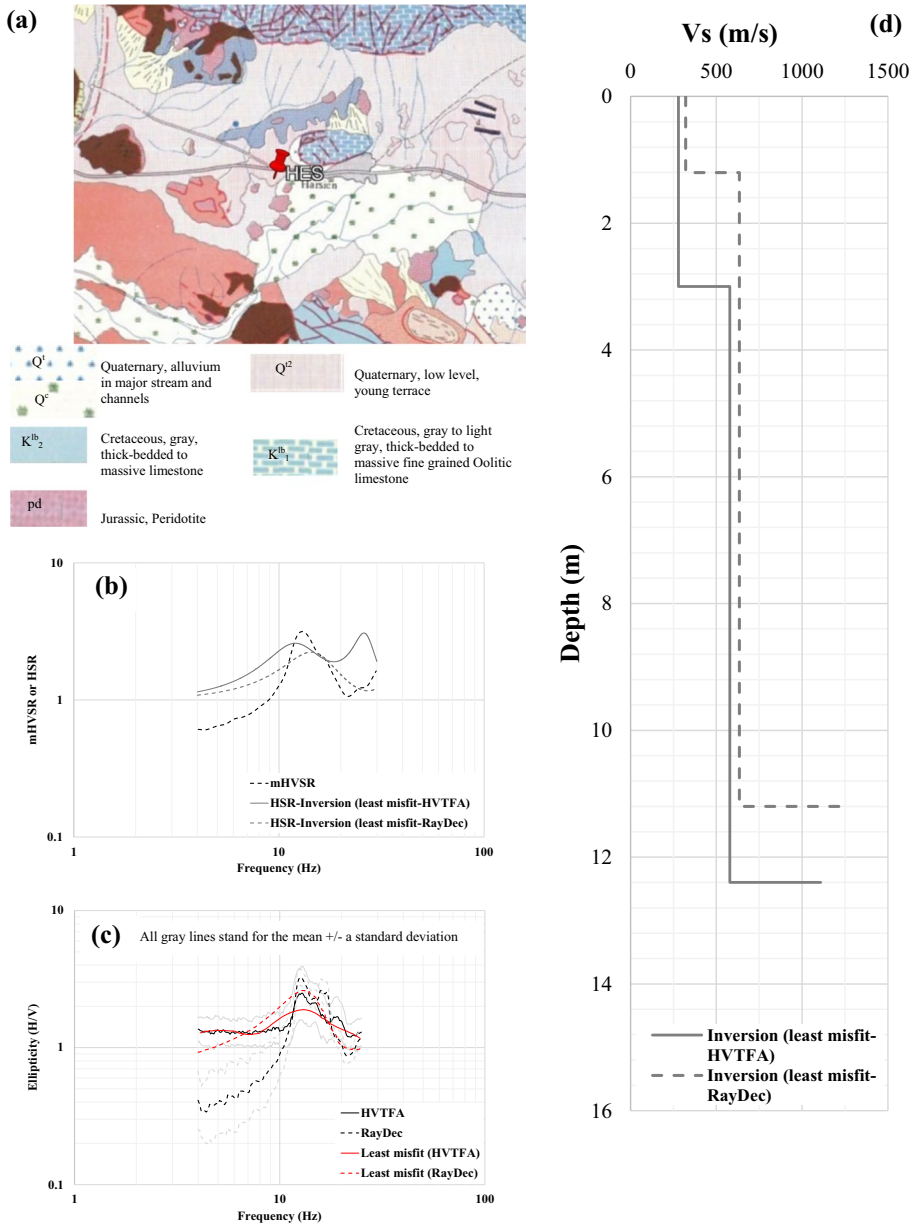


Fig. 7 Summary of HES Station: **a** Geological map, **b** mHVSr and HSR curves, **c** ellipticity curves of ambient noise by RayDec & HVTFa as well as the least misfit models, **d** V_s -profiles

result of the least misfit curve obtained from inversion of the ellipticity of ambient noise. As observed in Fig. 8c the ellipticity of the least misfit model properly fits to the observed ellipticity curve from ambient noise. The V_s -profile of the least misfit model is shown in Fig. 8d, and the HSR of the least misfit model is plotted in Fig. 8b for comparison with the

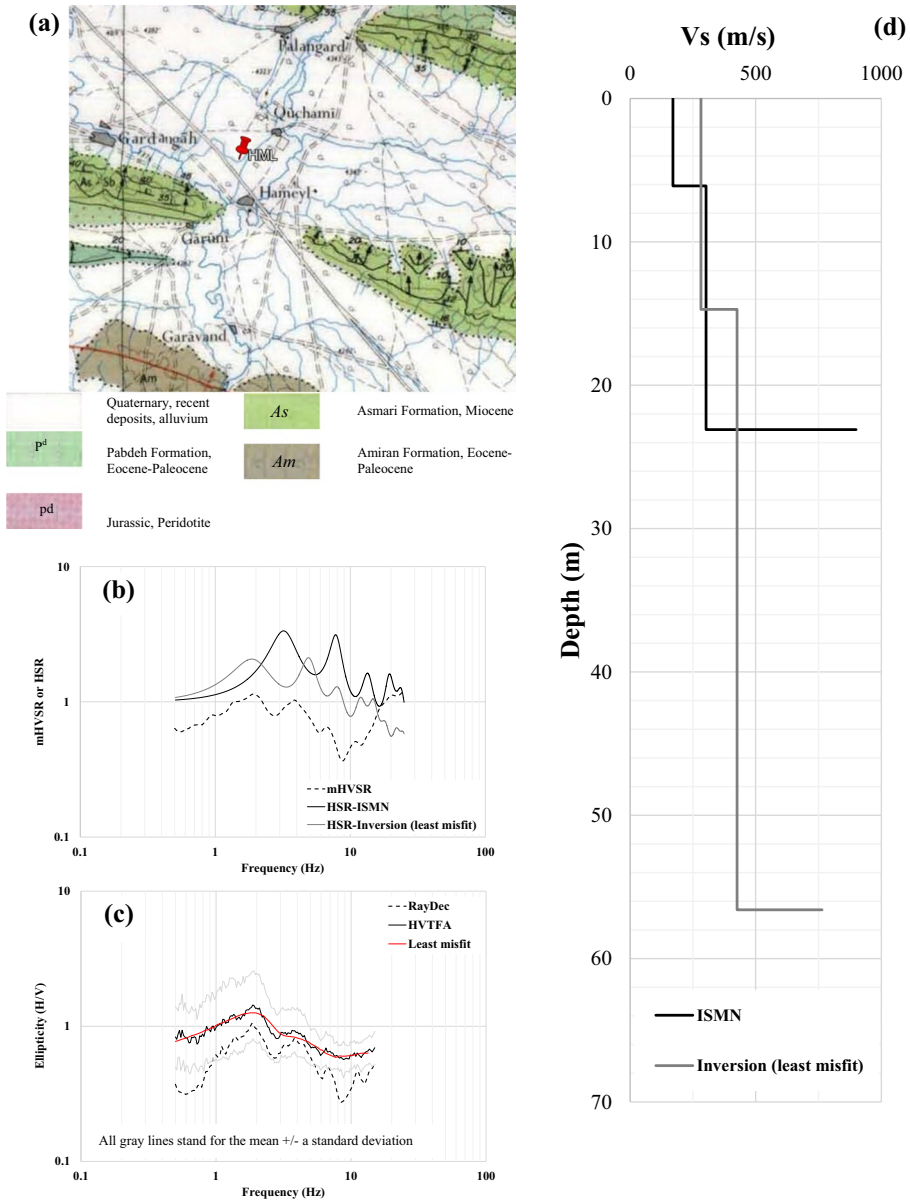


Fig. 8 Summary of HML Station: **a** Geological map, **b** mHVSr and HSR curves, **c** ellipticity curves of ambient noise by HVTFa & RayDec as well as the least misfit model, **d** Vs-profiles

ISMN profile and the HSR, respectively. Figure 8b shows that the frequency of peak amplitude of the HSR for the least misfit model is 1.9 Hz, almost identical to the mHVSr peak frequency. Inspecting Fig. 8d reveals that the ISMN profile is relatively consistent with the inverted profiles at the top 25 m but does not present a reasonable depth for the engineering bedrock layer that is about 55 m in the least misfit model. It should be noted that RayDec

method was used to retrieve the ellipticity curve at this station as is shown in Fig. 8c along with the other ellipticity curves, but the retrieved ellipticity barely presents amplitudes more than 1. Hence, the retrieved ellipticity was not used for velocity inversion analysis.

3.7 Station KRD

Figure 9a presents the location of this station on the geological map of the region on the young alluvial terrace of the Quaternary era. Figure 9d presents the V_S -profile provided in the ISMN database approximately 420 m northeast of the station's location, which might be affected by the Aghajary Formation. The V_S -profile shows relatively stiff ground 2.7 m thick ($V_S=307$ m/s) on top of a sharp velocity contrast with $V_S=948$ m/s down to a depth of 7.8 m that overlays a layer with $V_S=1152$ m/s. The close shear wave velocity of the second layer to the third layer suggests that it might be weathered, while well representing engineering bedrock. Figure 9b presents the ambient noise analyses of this station. It shows that the frequency of the peak amplitude of mHVSr is at 4.7 Hz (± 0.6). The V_S -profile of the ISMN database at this station (Fig. 9d) shows shallow bedrock ($V_S=948$ and 1152 m/s) at depths of 2.7 and 7.8 m, respectively. Figure 9b plots the HSR curve of the ISMN profile by considering two layers resting on an elastic half-space ($V_S=1152$ m/s), presenting the frequency of the peak at 25.3 Hz, and clearly inconsistent with the peak of mHVSr. The long distance between the station and logging location (i.e., 420 m) and the existence of other geological settings like the Aghajary Formation may have influenced the ISMN profile. The ellipticity of Rayleigh waves from HVTFA and RayDec methods are shown in Fig. 9c, and it is observed that the ellipticity curves of the both methods are very similar around the peak. Furthermore, Fig. 9c presents the ellipticity curves of the least misfit models of the inversion analysis. It is observed that the least misfit model for the inversion of ellipticity curve of HVTFA represents better the peak, while the one for the inversion of ellipticity curve of RayDec represents better the right flank of the ellipticity curve. Figure 9d presents V_S -profiles of the least misfit models along with the ISMN profile. It is observed that the ISMN profile is only consistent with the least misfit models at the top 3 m. Meanwhile, the least misfit models reveal that the young alluvium from the Quaternary era properly covers the bedrock beneath the station down to a depth of about 23 to 27 m. It is also shown that the least misfit models for the inversion of ellipticity curves of HVTFA and RayDec methods are reasonably consistent. Figure 9b plots the HSR curves for the least misfit models, showing the frequency of peak amplitude at 4.4 and 5.5 Hz for the least misfit ellipticity curves of HVTFA and RayDec methods, respectively, and clearly are matching with the frequency of peak from mHVSr.

3.8 Stations KRM1 & KRM2

Figures 10a and 11a present the locations of these stations on the geological map of the region. The two stations are about 3.5 km away from each other, and both are located on recent alluvium from the Quaternary era. A geological section is available about 2500 m and 900 m southeast of KRM1 and KRM2, respectively. This section shows that the Quaternary alluvium is thicker near KRM2 than KRM1. Unfortunately, no V_S -profiles were provided by the ISMN for these stations. However, inspecting Table 1 for the PGAs recorded at the 12 November 2017 earthquake event at these stations reveals the significantly different site effects at these stations (see also Ashayeri et al. 2019). Figure 10b,

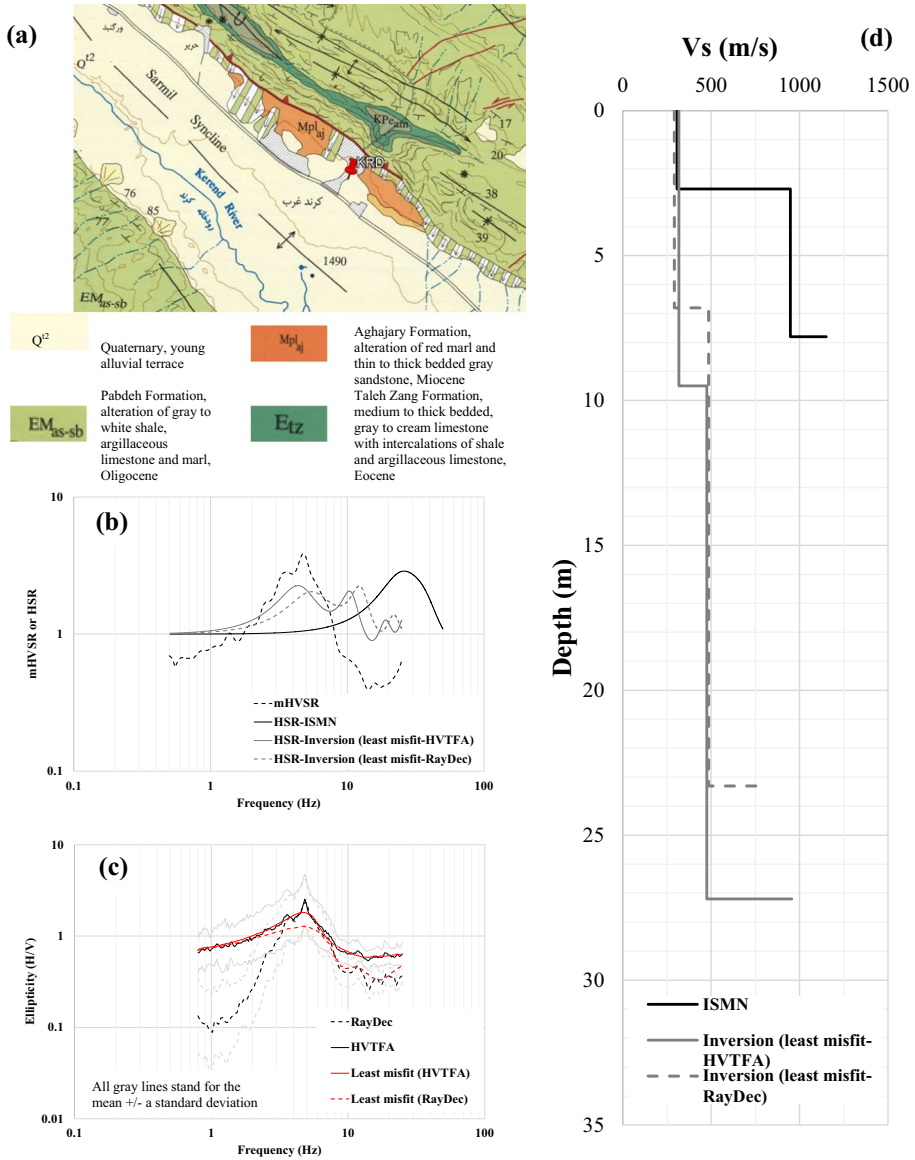


Fig. 9 Summary of KR D Station: **a** Geological map, **b** mHVSr and HSR curves, **c** ellipticity curves of ambient noise by RayDec & HVTFA as well as the least misfit models, **d** V_s -profiles

presenting ambient noise analyses of KRM1, shows that the frequency of the peak amplitude of mHVSr is 4.0 Hz (± 0.5) at KRM1.

The ellipticity of Rayleigh waves from HVTFA and RayDec methods are shown in Fig. 10c. The ellipticity curves of both methods are identical at frequencies higher than 3 Hz, which covers the peak frequency and the right flank of the ellipticity curve. The ellipticity of the least misfit models of inversion analysis are plotted in Fig. 10c, which

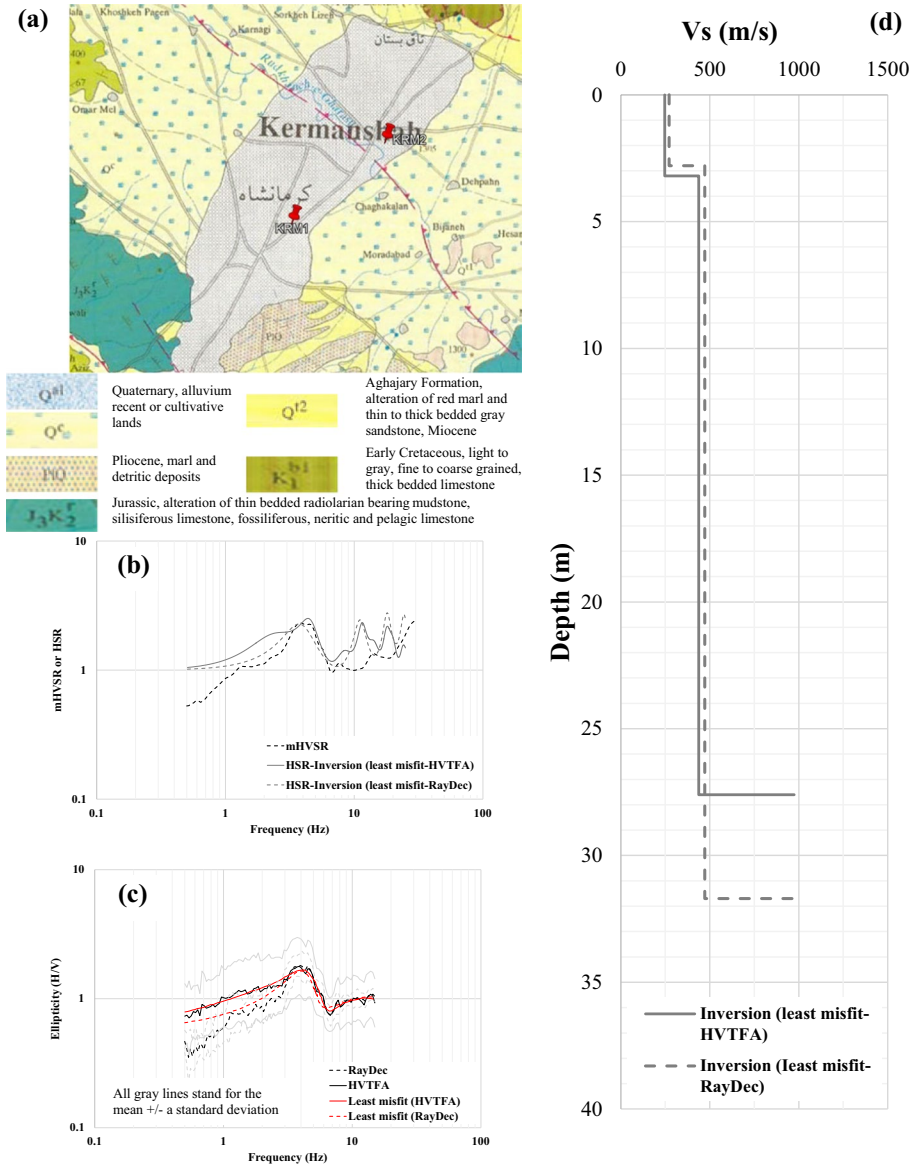


Fig. 10 Summary of KRM1 Station: **a** Geological map, **b** mHVSr and HSR curves, **c** ellipticity curves of ambient noise by RayDec & HVTFA as well as the least misfit models, **d** V_s -profiles

are perfectly matched with their targets at a wide range of frequencies. Figure 10b plots the HSR curves for the least misfit models, showing the frequency of the peak amplitude at 4.4 and 3.7 Hz for the least misfit models of ellipticity curves of HVTFA and RayDec methods, respectively. It is clearly observed that both match with the frequency of the peak from mHVSr. Figure 10d presents V_s -profiles of the least misfit models. It

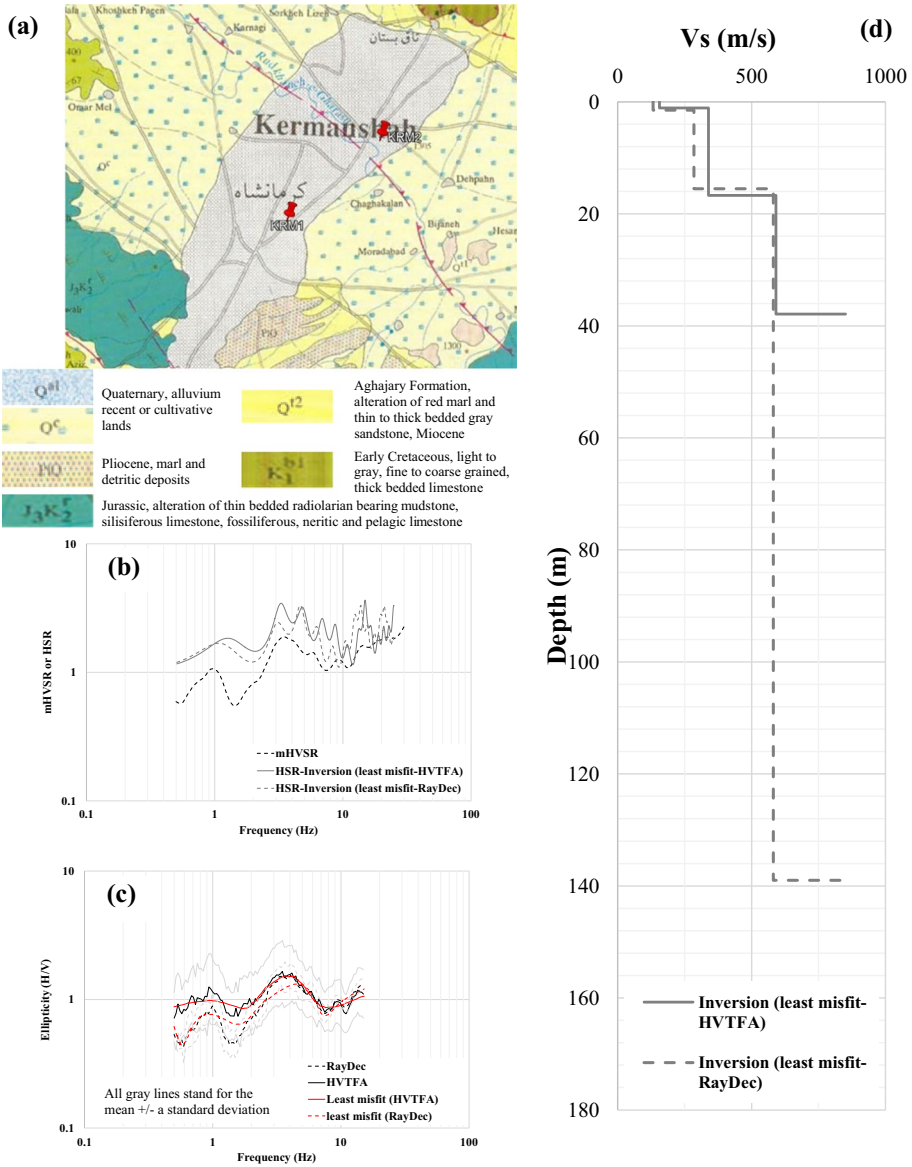


Fig. 11 Summary of KRM2 Station: **a** Geological map, **b** mHVSr and HSR curves, **c** ellipticity curves of ambient noise by RayDec & HVTFA as well as the least misfit models, **d** V_s -profiles

demonstrates that the thickness of the top layer is about 3 m with $V_s = 247$ to 271 m/s, covering thick and stiff soil with $V_s = 438$ to 471 m/s down to a depth of 28 to 32 m.

Figure 11b presents the ambient noise analyses of KRM2. It shows that the frequency of the peak amplitude of mHVSr is 3.7 Hz (± 0.5) at KRM2. It is worth noting that a lower frequency with a lower peak amplitude is observed at 0.94 Hz (± 0.13) on the mHVSr curve. The ellipticity of Rayleigh waves from HVTFA and RayDec methods

are shown in Fig. 11c. The ellipticity curves of both methods are identical at frequencies higher than 3 Hz but, there are differences in the amplitude of the ellipticity curves at lower frequencies. Furthermore, the peak frequency at about 1 Hz is represented better by the ellipticity curve of RayDec method. The ellipticity of the least misfit models of inversion analysis are shown in Fig. 11c, which are appropriately matched with their targets. Figure 11b plots the HSR curves for the least misfit models, showing the frequency of peak amplitude at 3.1 Hz for the both least misfit models, appropriately matching the peak frequency from mHVSr. Furthermore, the HSR curves for the least misfit models also show a lower frequency with a lower peak amplitude at 1.1 Hz, correspondingly matching the lower frequency peak of mHVSr. Figure 11d presents V_S -profiles of the least misfit models. It demonstrates that the two least misfit models have similar V_S -profiles down to a depth of 40 m, but the least misfit model of ellipticity of RayDec method presents deeper engineering bedrock at a depth of about 140 m. It is interpreted due to better representation of the ellipticity curve at lower frequencies than 3 Hz by the RayDec method.

3.9 Station MHD

Figure 12a presents the location of this station on the geological map of the region on a vast alluvial plain from the Quaternary era. A geological Sect. 2.9 km northwest of the station shows that the Quaternary alluvial plain is about 100 m thick and overlays the Amiran Formation. Figure 12d presents the V_S -profile provided by the ISMN database approximately 400 m south of the station's location. Although it is rather far away, there is no variation in the geological setting even at such a distance. The V_S -profile shows a relatively loose layer 3.6 m thick ($V_S=140$ m/s) on top of a stiffer layer down to a depth of 15.6 m ($V_S=361$ m/s), which overlays a layer with $V_S=460$ m/s. It is unclear how deep the third layer extends, and its V_S resembles stiff soil that is much looser than engineering bedrock ($V_S=750$ m/s). Figure 12b presents the ambient noise analyses of this station. It shows that the frequency of the peak amplitude of mHVSr is at 1.1 Hz (± 0.2), which is consistent with the fact that this station is located on loose and thick alluvial deposits from the Quaternary era (Fig. 12a). The V_S -profile from the ISMN database at this station did not end in a V_S comparable to engineering bedrock (see Fig. 12d), and therefore, it is not possible to calculate a reasonable HSR curve from the ISMN profile at MHD. The ellipticity of Rayleigh waves from HVTFA and RayDec methods are shown in Fig. 12c. It is observed that the two ellipticity curves are similar at frequencies lower than 1.5 Hz, but the ellipticity at higher frequencies are different in amplitude. With respect to the better performance of RayDec method, it is concluded that the right flank of the ellipticity curve is better represented by this method. The ellipticity of the least misfit models of inversion analysis are plotted in Fig. 12c, which are appropriately matched with their targets at a wide range of frequencies. However, the better representation of the right flank of ellipticity is observed in the least misfit model of RayDec method. Figure 12d presents V_S -profiles of the least misfit models along with the ISMN profile, which shows the ISMN profile is relatively consistent with the least misfit models at the top 16 m. However, the least misfit models reveal that engineering bedrock could be located at a depth of about 125 to 136 m with $V_S=886$ to 905 m/s. Figure 12b plots the HSR curve for the least misfit models, showing the frequency of the peak amplitude at 1.1 Hz, which is almost identical to the frequency of the peak from mHVSr.

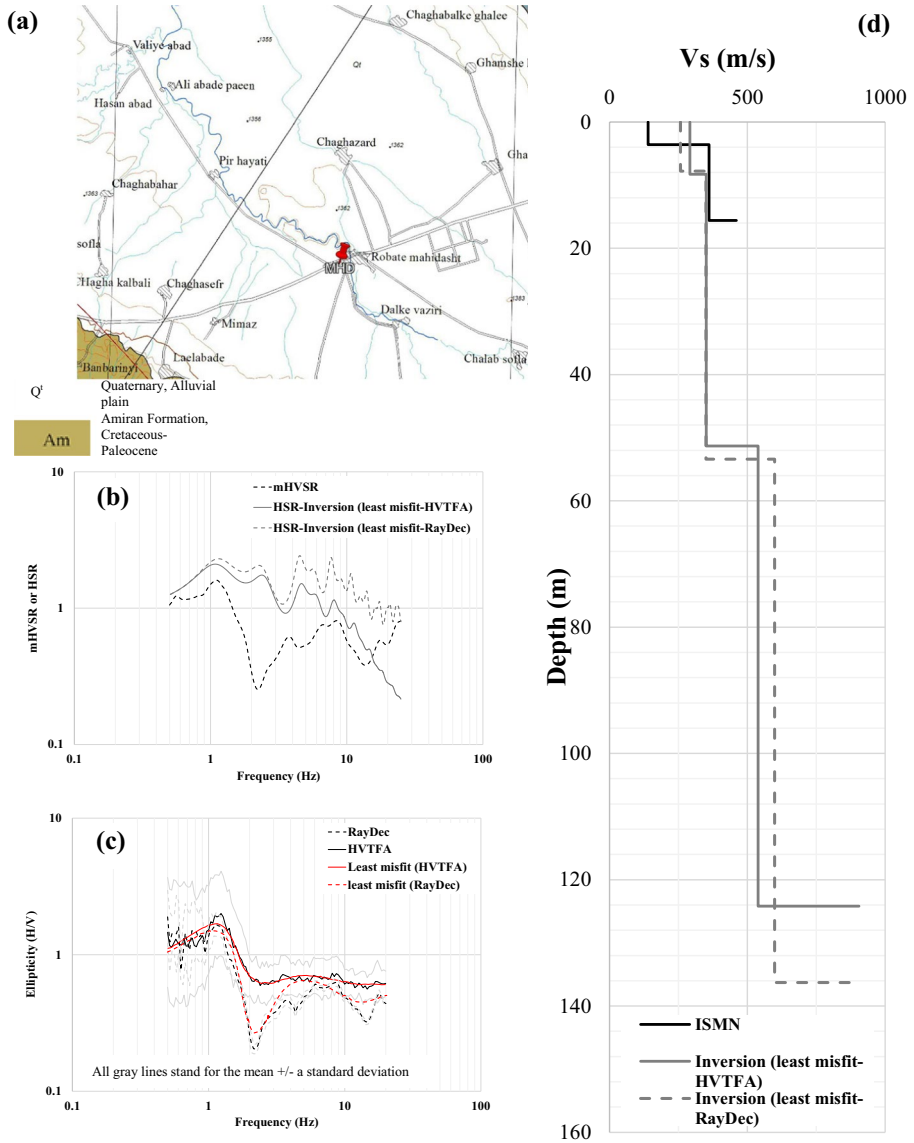


Fig. 12 Summary of MHD Station: **a** Geological map, **b** mHVSr and HSR curves, **c** ellipticity curves of ambient noise by RayDec & HVTFa as well as the least misfit models, **d** V_S -profiles

3.10 Station QSR

Figure 13a presents the location of this station on the geological map of the region. The station is located on the Aghajary Formation. Figure 13c presents the V_S -profile provided in the ISMN database approximately 385 m south of the station's location, which is rather far. The V_S -profile shows a loose layer 5.1 m thick ($V_S=110$ m/s) on top of a sharp velocity contrast down to a depth of 18.9 m ($V_S=622$ m/s), which overlays a layer with $V_S=970$ m/s. It is not

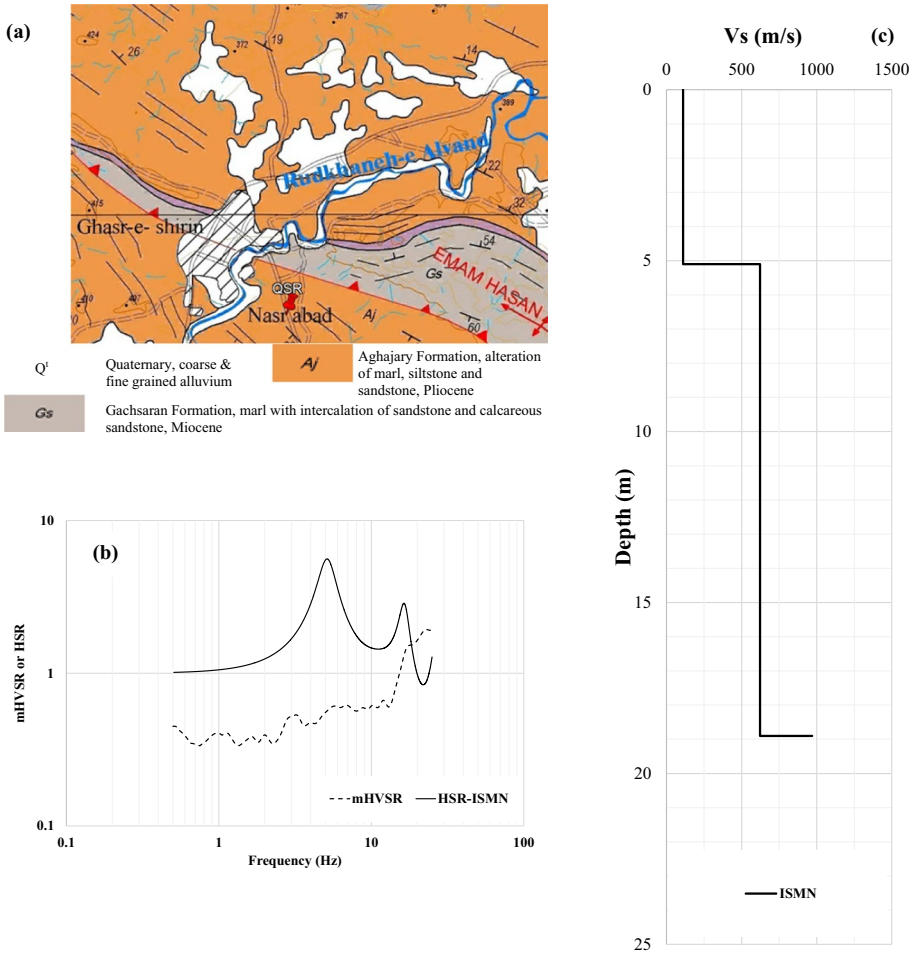


Fig. 13 Summary of QSR Station: **a** Geological map, **b** mHVSR and HSR curves, **c** V_s -profile

clear how deep the third layer extends, and its V_s resembles that of weathered rock, larger than the V_s of engineering bedrock ($V_s=750$ m/s). Figure 13b presents the mHVSR curve of the ambient noise records at QSR and shows no clear peak. Therefore, it is not possible to calculate the ellipticity curve of the ambient noise at this station. Figure 13b presents the HSR curve of the ISMN profile, showing a peak amplitude at 5.1 Hz. The authors conclude that the ISMN profile should be used with caution for Station QSR, and a more accurate profile should be measured by either direct borehole tests next to the station or more complex ambient noise and strong motion inversion methods in the future.

3.11 Station RVN

Figure 14a presents the location of this station on the geological map of the region on the alluvium of the Quaternary era. Figure 14c presents the V_s -profile provided by the

ISMN database approximately 500 m southeast of the station’s location, which is far. The V_S -profile shows a loose layer 4.5 m thick ($V_S = 105$ m/s) on top of a stiffer layer down to a depth of 16.5 m ($V_S = 368$ m/s), which overlays a layer with $V_S = 714$ m/s. It is unclear how deep the third layer extends, but its V_S resembles that of weathered rock comparable with the V_S of engineering bedrock ($V_S = 750$ m/s). Figure 14b presents the mHVSr curve of the ambient noise records at RVN, showing no clear peak. Therefore, it is not possible to calculate the ellipticity curve of the ambient noise at this station. Furthermore, Fig. 14b presents the HSR curve of the ISMN profile for RVN, showing a peak amplitude at 4.7 Hz. The authors conclude that the ISMN profile should be used with caution for RVN, and a more representative profile should be measured by either direct borehole tests next to the station or more complex ambient noise and strong motion inversion methods in the future.

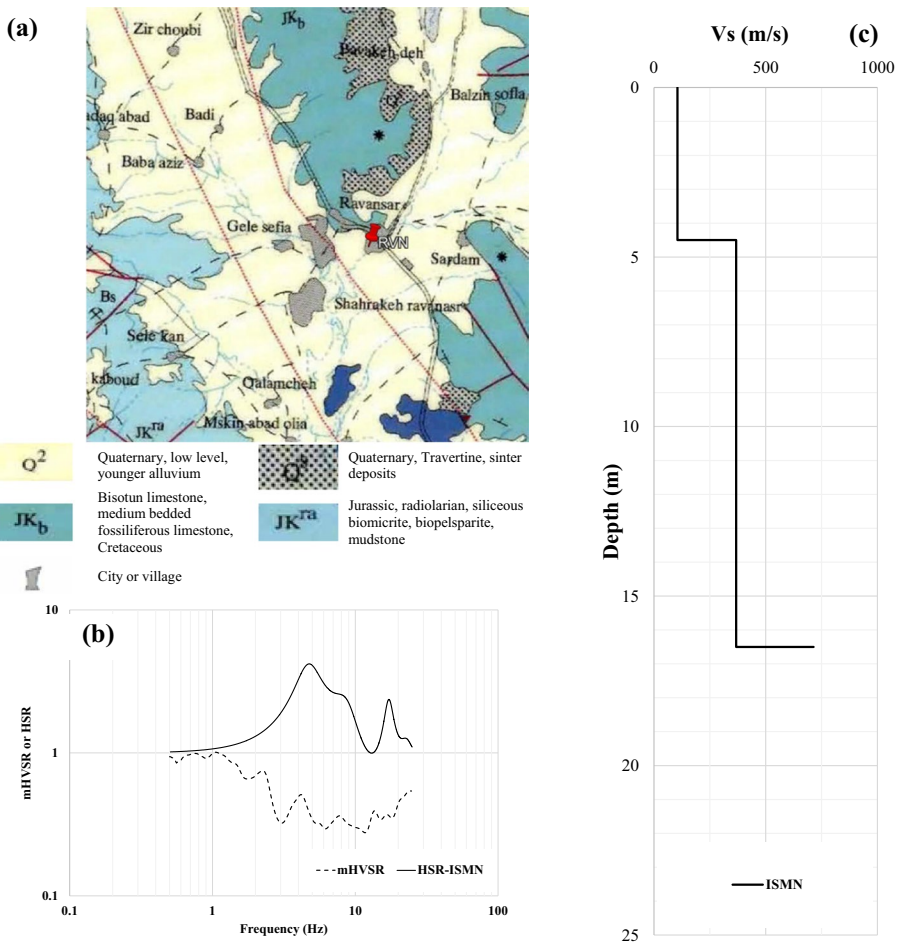


Fig. 14 Summary of RVN Station: **a** Geological map, **b** mHVSr and HSR curves, **c** V_S -profile

3.12 Station SLS

Figure 15a presents the location of this station on the geological map of the region. The station is located on the alluvial plain of the Quaternary era. Figure 15d presents the V_S -profile provided by the ISMN database approximately 700 m northwest of the station’s location. The V_S -profile shows a loose layer 4.7 m thick ($V_S=112$ m/s) on top of a stiff

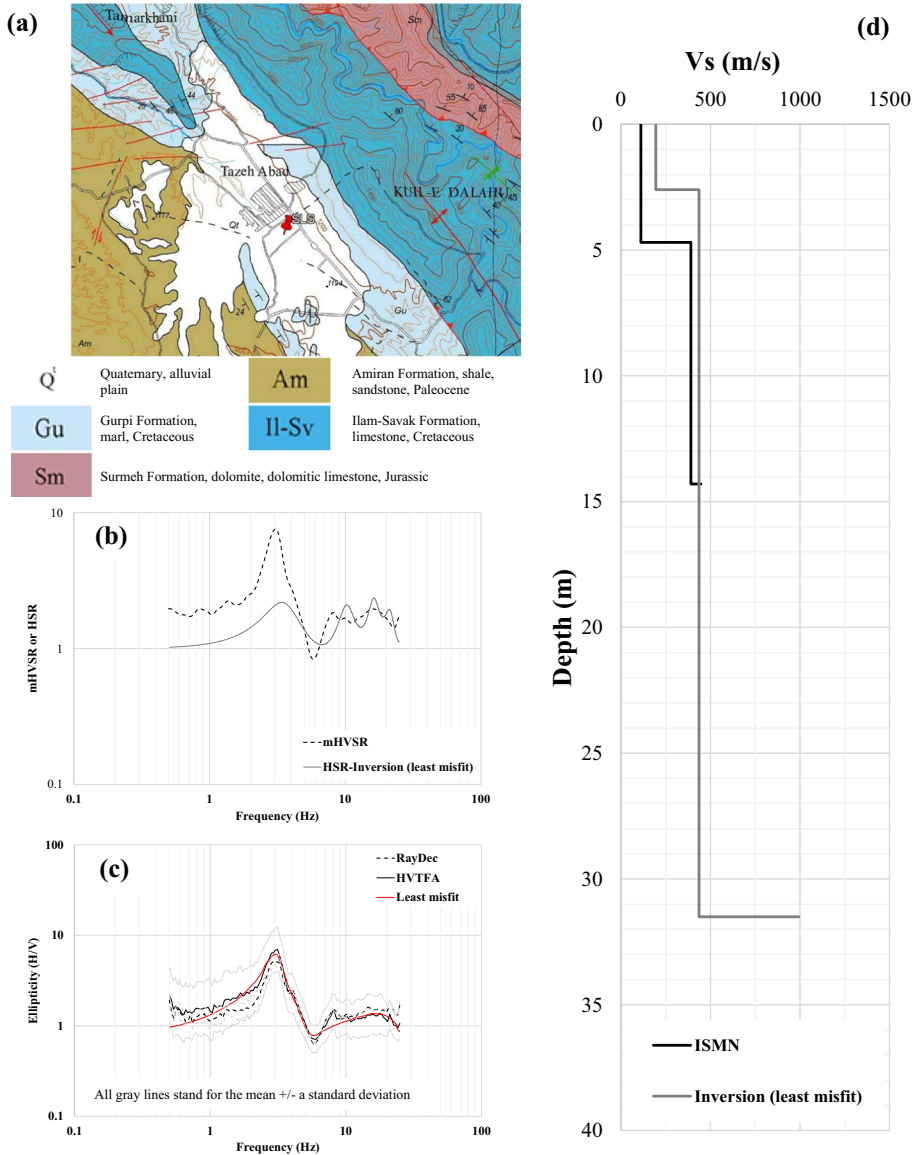


Fig. 15 Summary of SLS Station: **a** Geological map, **b** mHVSr and HSR curves, **c** ellipticity curves of ambient noise by RayDec & HVTFa as well as the least misfit model, **d** V_S -profiles

layer down to a depth of 14.3 m ($V_S=390$ m/s), which overlays a layer with $V_S=447$ m/s. It is unclear how deep the third layer extends, and its V_S resembles stiff soil that is much looser than engineering bedrock ($V_S=750$ m/s). Figure 15b presents the ambient noise analyses of this station. It shows that the peak amplitude of mHVSr is 3.1 Hz (± 0.1), which is consistent with the fact that this station is located on relatively thick and loose alluvial deposits of the Quaternary era (Fig. 15a). The V_S -profile of the ISMN database at this station did not end in the V_S of engineering bedrock (Fig. 15d), and therefore it is not possible to calculate a reasonable HSR curve from the ISMN profile at SLS. The ellipticity of Rayleigh waves from HVTFA and RayDec methods are shown in Fig. 15c. The two ellipticity curves are very similar at entire frequency range. The ellipticity of the least misfit model of inversion analysis, which is appropriately matched with the targets are shown in Fig. 15c. Figure 15d presents V_S -profiles of the least misfit model along with the ISMN profile, showing that the ISMN profile is properly consistent with the least misfit model at the top 16 m. However, the least misfit model reveals that engineering bedrock could be located at a depth of about 32 m with $V_S=994$ m/s. Figure 15b plots the HSR curve for the least misfit model, showing the frequency of the peak amplitude at 3.4 Hz, clearly matching with the peak frequency from mHVSr.

3.13 Station SNI

Figure 16a presents the location of this station on the geological map of the region on the alluvial plain of the Quaternary era. A geological section about 1250 m southwest of the station shows that the Quaternary alluvium is about 100 m thick. Figure 16d presents the V_S -profile provided by the ISMN database approximately 188 m west of the station's location. The V_S -profile shows a relatively loose layer 3.0 m thick ($V_S=180$ m/s) on top of a stiffer layer down to a depth of 18.0 m ($V_S=357$ m/s), which overlays a layer with $V_S=420$ m/s. It is unclear how deep the third layer extends, and its V_S resembles stiff soil that is much looser than engineering bedrock ($V_S=750$ m/s). Figure 16b presents the ambient noise analyses of the station. It shows that the frequency of the peak amplitude of mHVSr is at 4.1 Hz (± 0.7). The ISMN V_S -profile at this station did not end in the V_S of engineering bedrock (see Fig. 16d), and therefore it is not possible to calculate a reasonable HSR curve from the ISMN profile at SNI. The ellipticity of Rayleigh waves from HVTFA and RayDec methods are shown in Fig. 16c. It is observed that the two ellipticity curves are similar around the peaks of the ellipticity. However, the RayDec method presents better the left and right flanks of the ellipticity. The ellipticity curves of the least misfit models of inversion analysis are shown in Fig. 16c, which are appropriately matched with their targets. Figure 16d presents V_S -profiles of the least misfit models along with the ISMN profile, which shows the ISMN profile is perfectly identical to the least misfit models at the top 18 m. However, the least misfit models reveal that engineering bedrock may be located at a depth of about 23 m with $V_S=800$ m/s. Figure 16b plots the HSR curve for the least misfit models, showing the frequency of the peak amplitude at about 4.4 Hz, clearly matching with the frequency of the peak from mHVSr.

3.14 Station SON

Figure 17a presents the location of this station on the geological map of the region. The station is located on the lowest alluvial deposits of the Quaternary era. A geological section about 4 km northwest of the station shows that Eocene era rocks (E^V setting) underlie

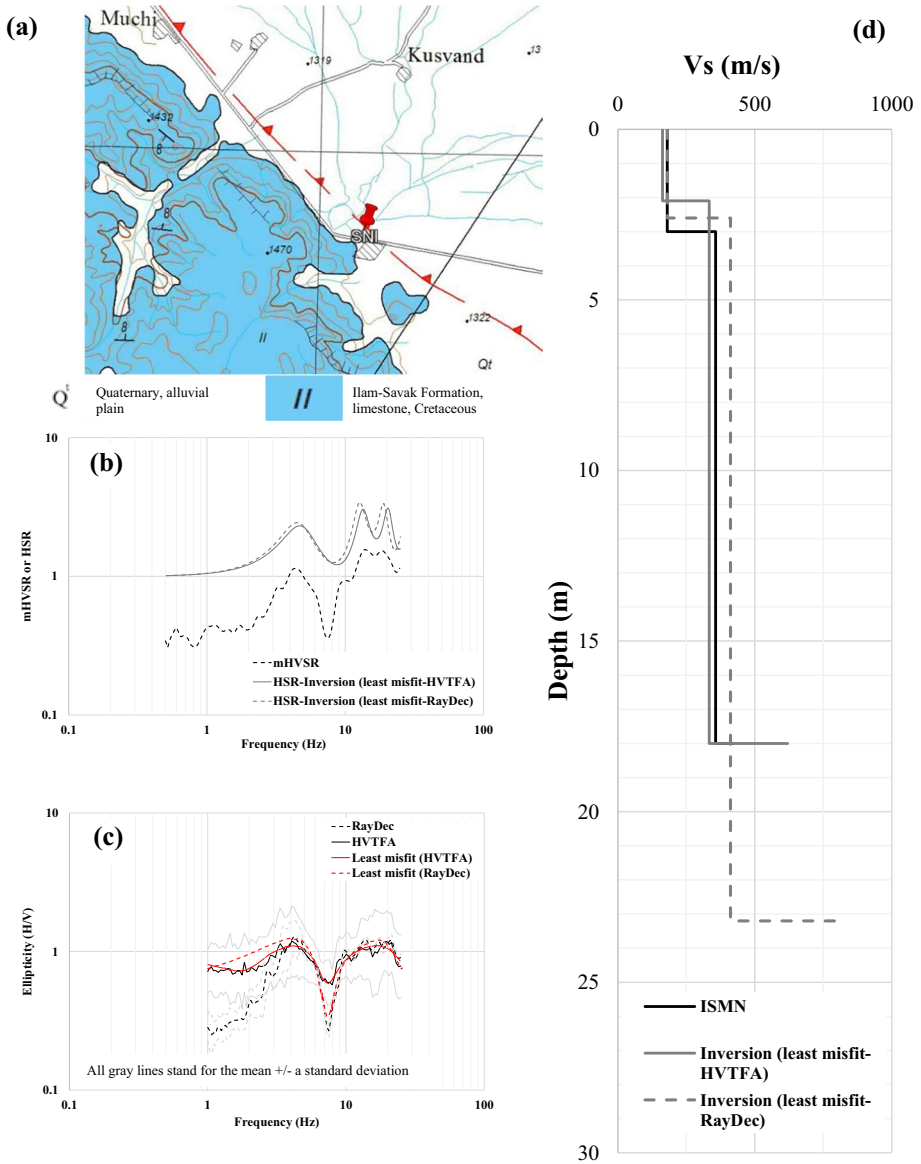


Fig. 16 Summary of SNI Station: **a** Geological map, **b** mHVSr and HSR curves, **c** ellipticity curves of ambient noise by RayDec & HVTFA as well as the least misfit models, **d** V_S -profiles

the thin Quaternary alluvium. Figure 17d presents the V_S -profile provided by the ISMN database about 400 m south of the station. The V_S -profile shows stiff ground 3.1 m thick ($V_S=655$ m/s) on top of a stiffer layer down to a depth of 9.1 m ($V_S=1671$ m/s), which overlays a layer with $V_S=1747$ m/s. It is unclear how deep the third layer extends, but the shear wave velocity of the first layer resembles that of weathered rock, and the V_S of the second layer is adequately larger than that of engineering bedrock ($V_S=750$ m/s).

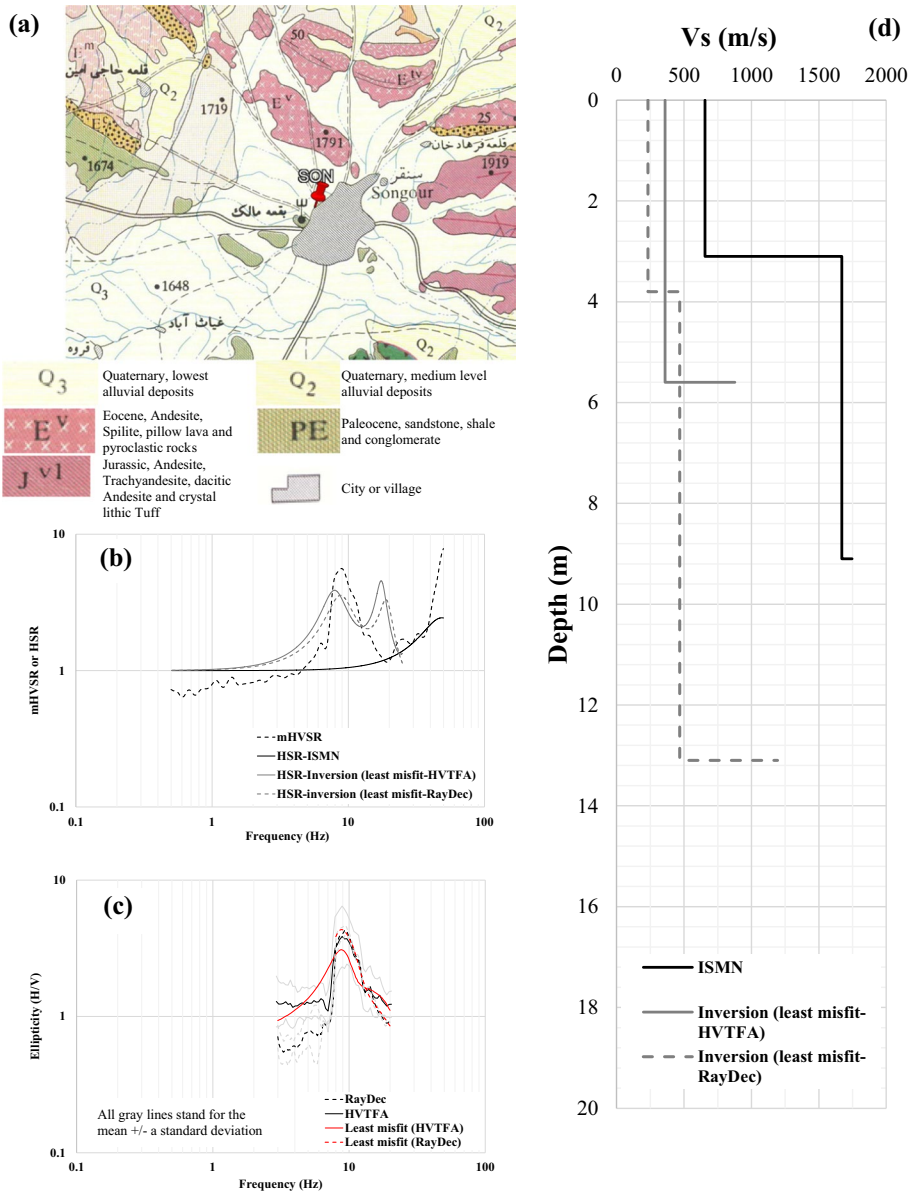


Fig. 17 Summary of SON Station: **a** Geological map, **b** mHVSR and HSR curves, **c** ellipticity curves of ambient noise by RayDec & HVTFA as well as the least misfit models, **d** V_S -profiles

Figure 17b presents the station’s ambient noise analyses, showing the frequency of the peak amplitude of mHVSR at 8.8 Hz (± 0.4). The ISMN V_S -profile at this station shows stiff ground on shallow competent bedrock ($V_S = 1671$ to 1747 m/s, see Fig. 17d). Hence, the calculated HSR curve from the ISMN profile in Fig. 17b shows no peak frequency less than 50 Hz. The ellipticity of Rayleigh waves from HVTFA and RayDec methods are

shown in Fig. 17c. The two ellipticity curves are very similar at frequencies higher than 7 Hz. The ellipticity curves of the least misfit models of inversion analysis are shown in Fig. 17c. It is observed that the least misfit model of ellipticity curve of RayDec method modelled better the peak amplitude and right flank of the ellipticity curve. Figure 17d presents V_S -profiles of the least misfit models along with the ISMN profile, which shows the ISMN profile presents larger velocities at all depths. With respect to better performance of the RayDec method, the least misfit model reveals that competent bedrock can be located at a depth of about 13 m with $V_S = 1194$ m/s. Figure 17b plots the HSR curve for the least misfit model that shows the frequency of the peak amplitude at 8.8 Hz, clearly matching with the frequency of the peak from mHVSr.

3.15 Station SPZ

Figure 18a presents the location of this station on the geological map of the region on the edge of Quaternary alluvium and consolidated conglomerate of the Bakhtyari Formation. Figure 18d presents the V_S -profile provided by the ISMN database approximately 500 m southeast of the station's location. This is important because the profile is relatively far from the station and may not represent the actual geological settings beneath the station. Nevertheless, the V_S -profile shows a relatively stiff layer 4.7 m thick ($V_S = 294$ m/s) on top of a sharp velocity contrast down to a depth of 14.1 m ($V_S = 779$ m/s), which overlays a layer with $V_S = 960$ m/s. It is unclear how deep the third layer extends, but the shear wave velocity of the second layer resembles weathered rock and is comparable with the V_S of engineering bedrock ($V_S = 750$ m/s). Figure 18b presents the ambient noise analyses of the station. It shows that the frequency of the peak amplitude of mHVSr is at 4.9 Hz (± 0.4). The ISMN V_S -profile at this station shows the engineering bedrock with $V_S = 779$ m/s (Fig. 18d). Hence, Fig. 18b presents the calculated HSR curve from the ISMN profile with the frequency of the peak amplitude at 13.5 Hz, clearly inconsistent with that of mHVSr. The ellipticity of Rayleigh waves from HVTFA and RayDec methods are shown in Fig. 18c. The two ellipticity curves are similar around the peak, but the RayDec method presents better curve at left and right flanks of the peak. The ellipticity curves of the least misfit models of inversion analysis are shown in Fig. 18c. Figure 18d presents V_S -profiles of the least misfit models along with the ISMN profile, which shows the ISMN profile presents larger velocities below a depth of 5 m. However, the least misfit models reveal that the engineering bedrock can be located at a depth of about 24 to 29 m with $V_S = 725$ to 810 m/s. Figure 18b plots the HSR curves for the least misfit models that show the frequencies of the peak amplitude at 4.7 and 6.3 Hz for the least misfit models of the ellipticity of HVTFA and RayDec, respectively that represent properly the peak from mHVSr.

3.16 Station SUM

Figure 19a presents the location of this station on the geological map of the region. The station is located on the plain of Quaternary alluvium. Figure 19d presents the V_S -profile provided by the ISMN database approximately 172 m east of the station's location. The V_S -profile shows relatively stiff ground 2.3 m thick ($V_S = 228$ m/s) on top of a sharp velocity contrast down to a depth of 15.0 m ($V_S = 754$ m/s), which overlays a layer with $V_S = 970$ m/s. It is unclear how deep the third layer extends, but the shear wave velocity of the second layer resembles weathered rock and is close to the V_S of engineering bedrock ($V_S = 750$ m/s). Figure 19b presents the ambient noise analyses of the station and

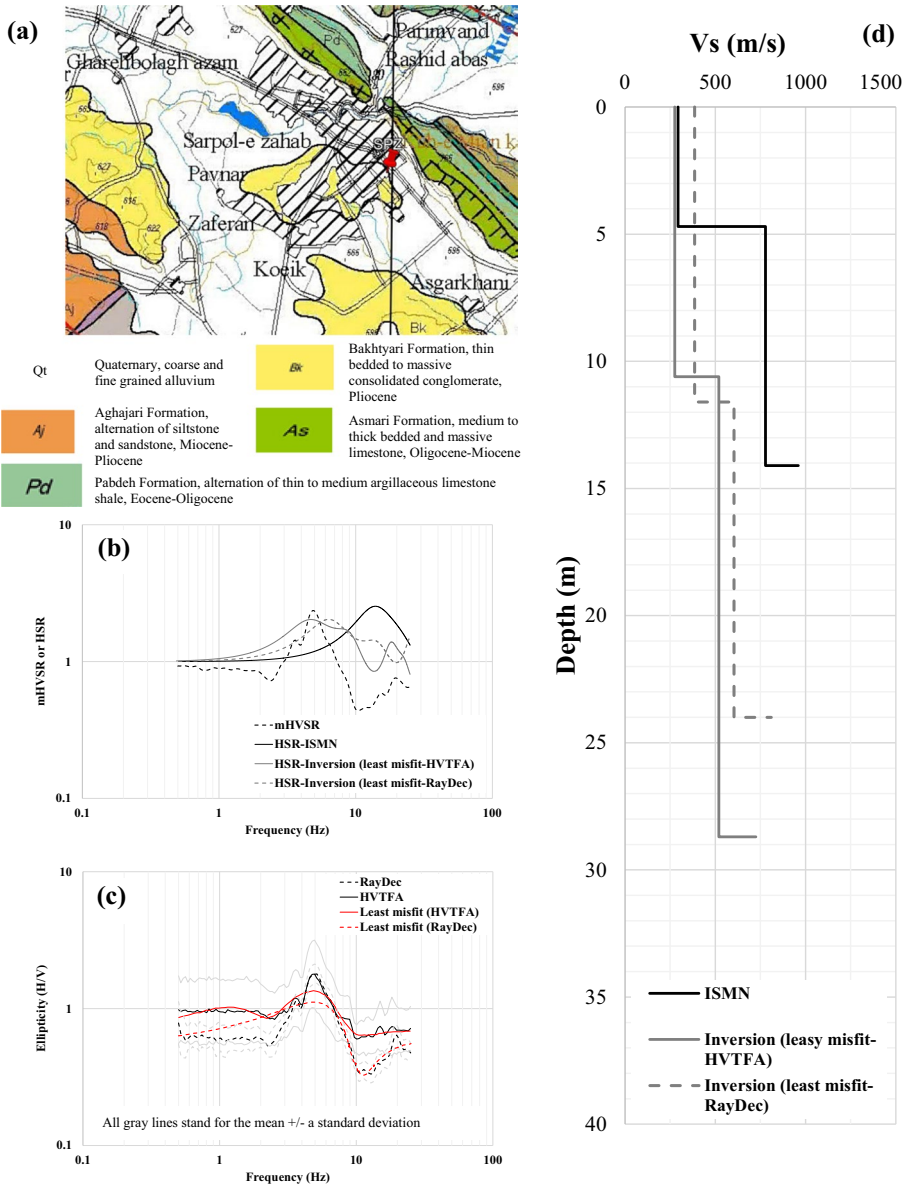


Fig. 18 Summary of SPZ Station: **a** Geological map, **b** mHVSr and HSR curves, **c** ellipticity curves of ambient noise by RayDec & HVTFA as well as the least misfit models, **d** V_s -profiles

shows that the frequency of the peak amplitude of mHVSr is at 4.1 Hz (± 0.7). The ISMN V_s -profile at this station shows engineering bedrock with $V_s = 754$ m/s (see Fig. 19d). Figure 19b presents the calculated HSR curve from the ISMN profile with the frequency of the peak amplitude at 25.5 Hz, clearly inconsistent with that of mHVSr. The ellipticity of Rayleigh waves from HVTFA and RayDec methods are shown in Fig. 19c. It is observed that the peak and right flank of the ellipticity are represented better by the RayDec method.

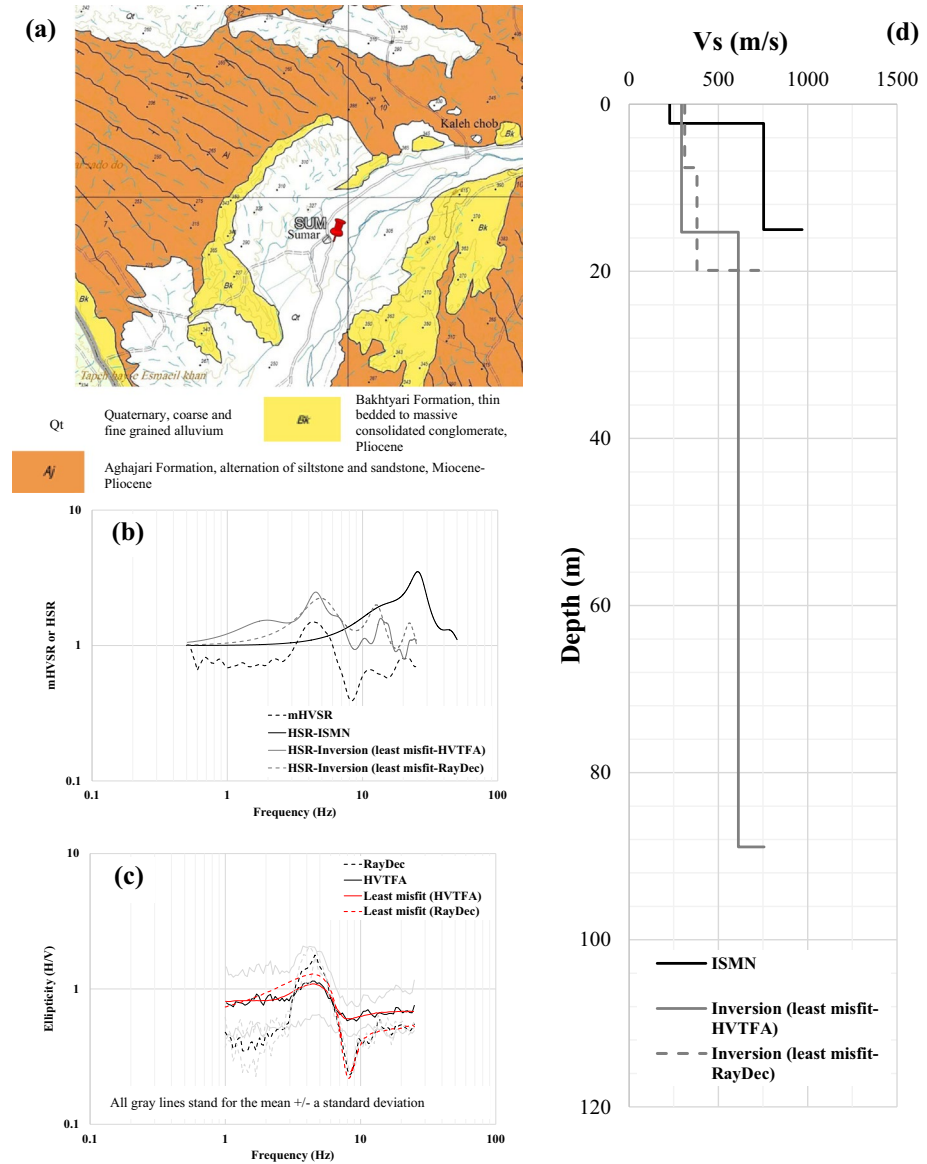


Fig. 19 Summary of SUM Station: **a** Geological map, **b** mHVSr and HSR curves, **c** ellipticity curves of ambient noise by RayDec & HVTFA as well as the least misfit models, **d** V_s -profiles

However, the ellipticity curves of the least misfit models of inversion analysis are plotted in Fig. 19c for the both methods. It is also observed that the least misfit model of the ellipticity of RayDec method is relatively more appropriate than the one of the HVTFA method. Figure 19d presents V_s -profiles of the least misfit models along with the ISMN profile, which shows the ISMN profile presents larger velocities below a depth of 3 m. However, with respect to better performance of the RayDec method, the least misfit model reveals

that the engineering bedrock may be located at a depth of about 20 m with $V_S = 726$ m/s. Figure 19b plots the HSR curves for the least misfit models, showing the frequency of the peak amplitude at about 5 Hz, properly matching with the frequency of the peak from mHVSR.

4 Discussion

This section presents some site proxies from the characteristics of V_S -profiles for the ISMN stations examined in this study (the V_S -profiles are available as electronic supplementary information). The site proxies are categorized into (i) geometry of layers, (ii) mechanical characteristics, and (iii) resonance frequencies. The geometry of layers is introduced by a group of parameters that describe the depth of layers in which $V_S \geq v$ m/s, namely Z_{Sv} . The mechanical characteristics are introduced by a group of parameters that describe the time-averaged shear wave velocity down to a depth in which $V_S \geq v$ m/s, namely V_{Sv} , and the time-averaged shear wave velocity of the top 30 m, i.e., $V_{S,30}$. Finally, the resonance frequencies are introduced by three parameters: (i) the lowest peak frequency in the mHVSR curve, i.e., $F_{0,mHVSR}$, (ii) the peak frequency in the mHVSR curve, i.e., $F_{P,mHVSR}$, and (iii) the first peak in the HSR curve, i.e., $F_{P,HSR}$. Obviously, $F_{0,mHVSR}$ and $F_{P,mHVSR}$ may be identical for some of the stations. Table 2 presents these site proxies for the stations examined in this study. Note that at four stations (i.e., GGH, CHN, RVN, and QSR), it was not possible to retrieve the subsurface structure from ambient noise analyses. Hence, some or all site proxies were measured using the ISMN's subsurface profiles.

As seen in Table 2, Z_{S400} and Z_{S700} are reported for all stations, representing the starting depth of stiff soil and engineering bedrock, respectively. However, in some stations, it is not possible to report Z_{S1500} , which represents the starting depth of competent bedrock. Table 2 presents a categorization of stations in terms of Z_{S700} for the depth of engineering bedrock as: (a) shallow, i.e., $Z_{S700} \leq 5$ m, (b) intermediate, i.e., $5 < Z_{S700} \leq 30$ m, (c) deep, i.e., $30 < Z_{S700} \leq 100$ m, (d) very deep, i.e., $Z_{S700} > 100$ m. It is worth noting that V_{S700} represents the time-averaged shear wave velocity of layers above the engineering bedrock at each station. It is observed that for sites with shallow engineering bedrock, V_{S700} is closer to V_{S400} and smaller than $V_{S,30}$, but V_{S700} is closer to $V_{S,30}$ and larger than V_{S400} in sites with intermediate engineering bedrock. Furthermore, in deep and very deep engineering bedrock, V_{S700} is larger than V_{S400} and $V_{S,30}$ and the two latter velocities are closer to each other.

A comparison between the engineering bedrock depth and the resonance frequency at each site reveals that the resonance frequency is lower as the engineering bedrock gets deeper. It should be noted that $F_{0,mHVSR}$, or $F_{P,HSR}$ in cases in which $F_{0,mHVSR}$ was not available, is considered as the resonance frequency. Figure 20 presents the equivalent site resonance frequencies, $F_{eq,v}$, in terms of the resonance frequency from ambient noise analysis. The equivalent site resonance frequencies are simply calculated from the site proxies and considering a homogeneous layer with the time-averaged shear wave velocity on a homogeneous half-space as Eq. 1.

$$F_{eq,v} = \frac{V_{Sv}}{4Z_{Sv}} \text{ or } \frac{V_{S,30}}{4 \times 30} \quad (1)$$

Therefore, two equivalent site resonance frequencies are calculated for soil layers with $V_S \leq 400$ and 700 m/s, and the third equivalent site resonance frequency is calculated from

Table 2 Summary of the site proxies of the stations

Station	Z _{S400} (m)	Z _{S700} (m)	Z _{S1500} (m)	V _{S400} (m/s)	V _{S700} (m/s)	V _{S30} (m/s)	F _{0,mHVS} R (Hz)	F _{1,mHVS} R (Hz)	F _{P,HSR} (Hz)	Engineer- ing bedrock depth ^b
GGH ^a	2	2	NA	150	150	692	NA	NA	16	Shallow
HES	1	11	22	321	574	939	13	13	14.3	Intermediate
SON	4	13	47	233	362	596	8.8	8.8	8.8	
CHN ^a	4	17	NA	169	353	419	5.8	5.8	9.5	
RVN ^a	17	17	NA	219	219	267	NA	NA	4.7	
QSR ^a	5	19	NA	110	276	403	NA	NA	5.1	
SUM	20	20	NA	350	350	424	4.1	4.1	5	
KRD	7	23	NA	292	407	454	4.7	4.7	5.5	
SNI	3	23	NA	181	360	411	4.1	17.5	4.4	
SPZ	12	24	NA	386	474	517	4.9	4.9	6.3	
SLS	3	31	111	194	393	392	3.1	3.1	3.4	Deep
KRM1	3	32	NA	271	442	441	3.9	3.9	3.7	
DIN	4	39	145	310	512	502	1.4	1.4	1.5	
HML	16	62	NA	311	414	368	1.9	1.9	1.9	
ELA	23	112	379	372	558	433	1.1	1.1	1.4	Very deep
MHD	53	136	NA	332	456	320	1.1	1.1	1.1	
KRM2	16	139	NA	256	509	350	0.9	3.7	1.1	

^aSome or all site proxies are reported from ISMN's PS-logs

^bReasoning based on Z_{S700}

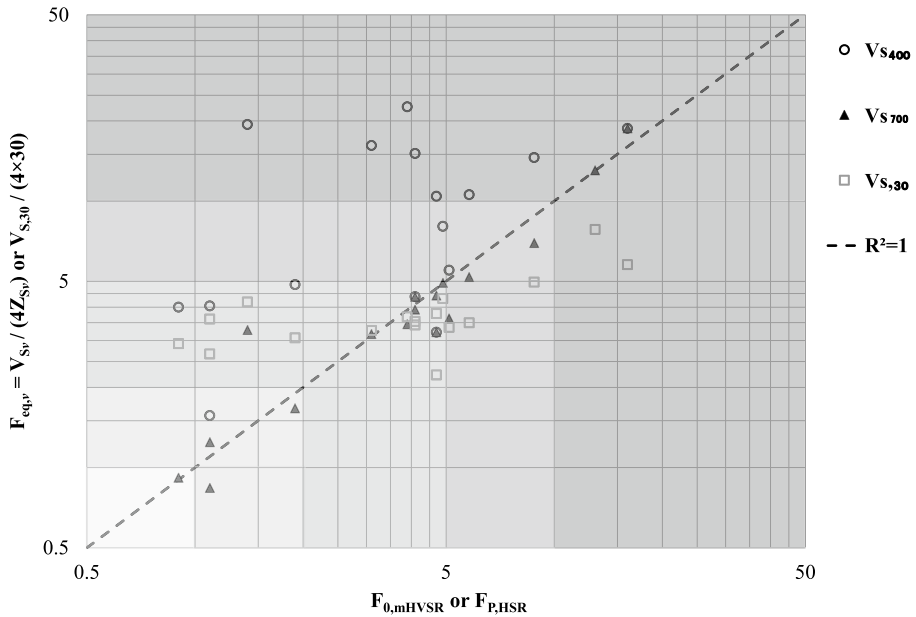


Fig. 20 Comparison between resonance frequencies from ambient noise analysis and equivalent site resonance frequencies

a column of 30 m depth at each site. It is observed that the equivalent site resonance frequency of the soil layers with $V_S \leq 700$, i.e., $F_{eq,700}$, shows the best consistency ($R^2 = 0.94$) with the resonance frequency of the ambient noise analysis. Meanwhile, it should be noted that there is no physical principle that the velocity contrast at Z_{S700} will make the resonance frequency of the ground. Furthermore, Fig. 20 shows the variation of the resonance frequency at each site by a gradient gray color as follows: (a) very low frequency where $F \leq 1$ Hz, (b) low frequency where $1 < F \leq 2$ Hz, (c) intermediate frequency where $2 < F \leq 5$ Hz, (d) high frequency where $5 < F \leq 10$ Hz, and (e) very high frequency where $F > 10$ Hz. In this categorization, all stations located on shallow engineering bedrock fall into very high resonance frequency class, all stations that are located on intermediate engineering bedrock fall into the intermediate to very high resonance frequency classes, and all stations that are located on deep and very deep engineering bedrock fall into the very low to intermediate resonance frequency classes. The comparison demonstrated in Fig. 20, basically shows that the single site proxy of $V_{S,30}$ (that is the only parameter in Iranian seismic code for the site classification), should be used with serious caution, and the authors like to encourage future investigations of the application of more site proxies like Table 2 as well as other research like Zhu et al. (2021) in the Iranian seismic code of practice.

5 Conclusions

This study provides a database for the site conditions of seventeen ISMN stations located in Kermanshah province based on geological surveys and ambient noise analyses. Ambient noise analyses of mHVSr, HVTFA, and RayDec were performed to obtain the resonance frequency

and ellipticity of Rayleigh waves at these sites. Furthermore, joint inversion of the ellipticity curve and resonance frequency for shear wave velocity profiles, and 1D-linear elastic modeling of V_S -profiles were carried out. Finally, the site proxies at these stations were reported in the three categories of (i) geometry of layers, (ii) mechanical characteristics, and (iii) resonance frequency. The authors draw the following conclusions from this study.

- (1) The ISMN database provided PS-logs of surface layers at 14 stations, but the logging location at these sites ranged from 137 to 700 m (except for DIN that was 10 m) away from the stations' location. These distances are rather large and, in some cases, misleading because of the geological lateral variability of the ground structure.
- (2) Ambient noise analyses successfully and suitably retrieved the site conditions in 13 stations but failed in 4 stations. The authors recommend direct borehole tests next to the stations or more complex ambient noise and strong motion inversion methods for these four stations.
- (3) Except for three stations (i.e., ELA, and SNI), the calculated V_S -profiles for the other stations from the inversion of ellipticity curves and resonance frequencies showed that the depths of engineering bedrock and/or competent bedrock were not reasonably represented in the ISMN V_S -profiles.
- (4) A set of useful and more representative site proxies, which are also introduced in recent investigations, were presented for the sites of the stations. In this way, the stations were categorized in terms of the depth of engineering bedrock and resonance frequency, and it was observed that Z_{S700} , V_{S700} , and resonance frequency had better correlations with each other at the sites of these stations.

Supplementary Information The online version contains supplementary material available at <https://doi.org/10.1007/s10518-022-01370-7>.

Acknowledgements We thank Razi University and the Road, Housing, and Urban Development Research Center for facilitating the collaboration of the authors in this study. Furthermore, the authors wish to acknowledge the anonymous reviewers for their instructive comments during the processing of the manuscript.

Author contributions Conceptualization: IA. Methodology: IA. Formal analysis and investigation: IA, MPS, AM. Writing—original draft preparation: IA. Writing—review and editing: IA, MPS. Resources: IA. Supervision: IA, MPS.

Funding No Funding.

Availability of data and material Not Applicable.

Code availability Not Applicable.

Declarations

Conflict of interest No conflicts of interest.

References

Ashayeri I, Biglari M, Sadr A, Haghshenas E (2019) Importance of revisiting $(V_S)_{30}$ site class index, Sarpol-e-zahab Mw=7.3 earthquake, earthquake geotechnical engineering for protection and development of

- environment and constructions—proceedings of the 7th international conference on earthquake geo-technical engineering, 17–20 June, 2019, Rome, Italy, pp 1194–1203
- Ashayeri I, Sadr A, Biglari M, Haghshenas E (2020) Comprehensive ambient noise analyses for seismic microzonation of sarpole-zahab after the Mw 7.3 2017 Iran earthquake. *Eng Geol.* <https://doi.org/10.1016/j.enggeo.2020.105636>
- Ashayeri I, Memari MA, Haghshenas E (2021) Seismic microzonation of Sarpol-e-zahab after Mw 7.3 2017 Iran earthquake: 1D-equivalent linear approach. *Bull Earthq Eng* 19:605–622. <https://doi.org/10.1007/s10518-020-00999-6>
- Bonnefoy-Claudet S, Köhler A, Cornou C, Wathelet M, Bard PY (2008) Effects of love waves on micro-tremor H/V ratio. *Bull Seismol Soc Am* 98(1):288–300. <https://doi.org/10.1785/0120070063>
- Cultrera G, Cornou C, Di Giulio G, Bard PY (2021) Indicators for site characterization at seismic station: recommendation from a dedicated survey. *Bull Earthq Eng* 19:4171–4195. <https://doi.org/10.1007/s10518-021-01136-7>
- Di Giulio G, Savvaidis A, Ohrnberger M, Wathelet M, Cornou C, Knapmeyer-Endrun B, Renalier F, Theodoulidis N, Bard PY (2012) Exploring the model space and ranking a best class of models in surface-wave dispersion inversion: application at European strong-motion sites. *Geophysics* 77(3):B147–B166. <https://doi.org/10.1190/geo2011-0116.1>
- Di Giulio G, Cultrera G, Cornou C, Bard PY, Al Tfaily B (2021) Quality assessment for site characterization at seismic stations. *Bull Earthquake Eng* 19:4643–4691. <https://doi.org/10.1007/s10518-021-01137-6>
- Fäh D, Wathelet M, Kristekova M, Havenith H, Endrun B, Stamm G, Poggi V, Burjanek J, Cornou C (2009) Using ellipticity information for site characterization, NERIES deliverable JRA4-D4
- Foti S, Parolai S, Bergamo P, Di Giulio G, Maraschini M, Milana G, Picozzi M, Puglia R (2011) Surface wave surveys for seismic site characterization of accelerometric stations in ITACA. *Bull Earthq Eng* 9:1797–1820. <https://doi.org/10.1007/s10518-011-9306-y>
- Garofalo F, Foti S, Hollender F, Bard PY, Cornou C, Cox BR, Ohrnberger M, Sicilia D, Asten M, Di Giulio G, Forbriger T, Guillier B, Hayashi K, Martin A, Matsushima S, Mercerat D, Poggi V, Yamanaka H (2016a) InterPACIFIC project: comparison of invasive and non-invasive methods for seismic site characterization. Part I: intra-comparison of surface wave methods. *Soil Dyn Earthq Eng* 82:222–240. <https://doi.org/10.1016/j.soildyn.2015.12.010>
- Garofalo F, Foti S, Hollender F, Bard PY, Cornou C, Cox BR, Dechamp A, Ohrnberger M, Perron V, Sicilia D, Teague D, Vergnault C (2016b) InterPACIFIC project: comparison of invasive and non-invasive methods for seismic site characterization. Part II: inter-comparison between surface-wave and borehole methods. *Soil Dyn Earthq Eng* 82:241–254. <https://doi.org/10.1016/j.soildyn.2015.12.009>
- Geological Survey of Iran (GSI). <https://www.gsi.ir/>
- Github (2021) Hobiger M. <https://github.com/ManuelHobiger/RayDec>
- Hashash YMA, Musgrove MI, Harmon JA, Groholski DR, Phillips CA, Park D (2016) DEEPSOIL 6.1, User Manual
- Hessami K, Jamali F, Tabassi H (2003) Major active faults of Iran. International Institute of Earthquake Engineering and Seismology (IIEES), Tehran, Iran
- Hobiger M, Bard PY, Cornou C, Le Bihan N (2009) Single station determination of Rayleigh wave ellipticity by using the random decrement technique (RayDec). *Geophys Res Lett* 36:L14303. <https://doi.org/10.1029/2009GL038863>
- Hobiger M, Cornou C, Wathelet M, Di Giulio G, Knapmeyer-Endrun B, Renalier F, Bard PY, Savvaidis A, Hailemikael S, Le Bihan N, Ohrnberger M, Theodoulidis N (2013) Ground structure imaging by inversions of Rayleigh wave ellipticity: sensitivity analysis and application to European strong-motion sites. *Geophys J Int* 192(1):207–229. <https://doi.org/10.1093/gji/ggs005>
- Homke S, Vergés J, Serra-Kiel J, Bernaola G, Sharp I, Garcés M, Montero-Verdú I, Karpuz R, Goodarzi MH (2009) Late Cretaceous–Paleocene formation of the proto–Zagros foreland basin, Lurestan Province, SW Iran *GSA Bulletin* 121(7–8):963–978. <https://doi.org/10.1130/B26035.1>
- National Iranian Oil Company (NIOC). <https://www.nioc.ir/>
- National Research Institute for Earth Science and Disaster Prevention (NIED). <https://www.kyoshin.bosai.go.jp/>
- National Road, Housing & Urban Development Research Center (BHRC). <https://ismn.bhrc.ac.ir/>
- Pilz M, Parolai S, Leyton F, Campos J, Zschau J (2009) A comparison of site response techniques using earthquake data and ambient seismic noise analysis in the large urban areas of Santiago de Chile. *Geophys J Int* 178:713–728. <https://doi.org/10.1111/j.1365-246X.2009.04195.x>
- Shahvar MP, Farzanegan E, Eshaghi A, Mirzaei H (2021) i1-net: The Iran strong motion network. *Seismol Res Lett* 92(4):2100–2108. <https://doi.org/10.1785/0220200417>
- Wathelet M (2008) An improved neighborhood algorithm: parameter conditions and dynamic scaling. *Geophys Res Lett* 35:1–5

- Wathelet M, Chatelian JL, Cornou C, Di Giulio G, Guilier B, Ohrnberger M, Savvaidis A (2020) Geopsy: a user-friendly open-source tool set for ambient vibration processing. *Seismol Res Lett* 91:1878–1889. <https://doi.org/10.1785/0220190360>
- Zhu C, Pilz M, Cotton F (2020) Which is a better proxy, site period or depth to bedrock, in modelling linear site response in addition to the average shear-wave velocity? *Bull Earthq Eng* 18:797–820. <https://doi.org/10.1007/s10518-019-00738-6>
- Zhu C, Weatherill G, Cotton F, Pilz M, Kwak DY, Kawase H (2021) An open-source site database of strong-motion stations in Japan: K-NET and KiK-net (v1.0.0). *Earthq Spectra* 37(3):2126–2149. <https://doi.org/10.1177/8755293020988028>

Publisher's Note Springer Nature remains neutral with regard to jurisdictional claims in published maps and institutional affiliations.